

ornl

ORNL/TM-11547



3 4456 0349407 4

**OAK RIDGE
NATIONAL
LABORATORY**

MARTIN MARIETTA

Resonance Analysis and Evaluation of the ^{235}U Neutron Induced Cross Sections

L. C. Leal

OAK RIDGE NATIONAL LABORATORY

CENTRAL RESEARCH LIBRARY

CIRCULATION SECTION

ADMIN. ROOM 173

LIBRARY LOAN COPY

DO NOT TRANSFER TO ANOTHER PERSON

If you wish someone else to see this
report, send its name with report and
the library will arrange a loan.

OPERATED BY
MARTIN MARIETTA ENERGY SYSTEMS, INC.
FOR THE UNITED STATES
DEPARTMENT OF ENERGY

This report is available directly from the best available source.

Available to DOE and DOE contractors from the Office of Scientific and Technical Information, P.O. Box 62, Oak Ridge, TN 37831; prices available from (615) 576-8401. FTS 920 8401.

Available to the public from the National Technical Information Service, U.S. Department of Commerce, 5285 Port Royal Rd., Springfield, VA 22161.
NTIS phone codes—Printed Copy: A30 Microfilm: M07

This report was prepared as an account of work sponsored by an agency of the United States Government. Neither the United States Government nor any agency thereof, nor any of their employees, makes any warranty, express or implied, or assumes any legal liability or responsibility for the accuracy, completeness, or usefulness of any information, apparatus, product, or process disclosed, or represents that its use would not infringe privately owned rights. Reference herein to any specific commercial product, process, or service by trade name, trademark, manufacturer, or otherwise, does not necessarily constitute or imply its endorsement, recommendation, or favoring by the United States Government or any agency thereof. The views and opinions of authors expressed herein do not necessarily state or reflect those of the United States Government or any agency thereof.

ORNL/TM-11547

Engineering Physics and Mathematics Division

RESONANCE ANALYSIS AND EVALUATION OF
THE ^{235}U NEUTRON INDUCED CROSS SECTIONS*

L. C. Leal

DATE PUBLISHED — June 1990

*Ph.D. Dissertation, University of Tennessee, Knoxville

Prepared for the
Office of Energy Research
Division of Nuclear Physics

Prepared by the
OAK RIDGE NATIONAL LABORATORY
Oak Ridge, Tennessee 37831
operated by
MARTIN MARIETTA ENERGY SYSTEMS, INC.
for the
U.S. DEPARTMENT OF ENERGY
under contract DE-AC05-84OR21400

MARTIN MARIETTA ENERGY SYSTEMS LIBRARIES



3 4456 0349407 4

ACKNOWLEDGMENTS

The author would like to express his appreciation to the people who contributed to various steps of this work: Dr. R. B. Perez who supervised the work and was the author's major professor, Dr. G. de Saussure of Oak Ridge National Laboratory for the stimulating discussions on the subject of the thesis and for his invaluable help, Drs. H. L. Dodds Jr. and B. R. Upadhyaya of the Nuclear Engineering Department, Dr. D. D. Bruns of the Chemical Engineering Department, Dr. F. C. Difilippo of Oak Ridge National Laboratory, and Dr. R. N. Hwang of Argonne National Laboratory for participating on the Committee.

The author also wishes to thank Dr. M. S. Moore of Los Alamos National Laboratory, Dr. N. M. Larson, Dr. F. G. Perey, Mrs. C. M. Perey, Mr. J. G. Craven, Dr. R. W. Peelle, and the ORELA staff for many helpful suggestions. Special thanks are extended to Dr. R. N. Hwang of Argonne National Laboratory for his advice concerning the Doppler broadening of cross sections method. Thanks are also due to Dr. T. W. Kerlin, head of the Nuclear Engineering Department of The University of Tennessee.

The author is indebted to Mrs. Sue Damewood for her assistance in typing and preparing the thesis.

Finally, the author thanks Conselho Nacional de Pesquisa (CNPq) of Brazil for support of this work, and Dr. S. L. Whetstone, DOE-Washington, for his support through the University Support Program of the U.S. Department of Energy.

TABLE OF CONTENTS

CHAPTER	PAGE
I. INTRODUCTION	1
1.0 Background	2
1.1 Need for the present work	3
1.2 Objectives	4
1.3 Organization of the dissertation	5
1.4 Accomplishments	6
II. RESONANCE THEORY	8
2.0 Overview of <i>R</i> -matrix theory	9
2.1 Reduced <i>R</i> -matrix formalism (Reich-Moore Formalism)	16
2.2 Adler-Adler formalism	19
2.3 Expansion of the collision matrix in momentum space	21
2.4 Theoretical statistical distribution of the resonance parameters	22
III. EXPERIMENTAL EFFECTS	24
3.0 Doppler broadening	24
3.1 A finite difference method for treating the Doppler broadening of cross sections	26
3.2 Resolution broadening	31
3.3 Normalization and residual background	31
IV. METHOD OF EVALUATION	33
4.0 Selection of data	34
4.1 Data reduction	36
4.2 Resonance analysis	38
V. RESULTS OF THE ANALYSIS	40
5.0 Graphical and tabular comparison with the data	41
5.1 Distribution of the resonance parameters	61
5.2 Comparison of the resolved and unresolved formalisms	68
VI. CONCLUSIONS AND RECOMMENDATIONS	72
LIST OF REFERENCES	75

CHAPTER	PAGE
APPENDICES	80
Appendix A. Relationship between Matrices \mathbf{U} , \mathbf{R} , and \mathbf{A}	81
Appendix B. Reich-Moore and Adler-Adler Neutron Cross-Section Formalism	83
Appendix C. Resonance Parameters for the Three Representations	85
Appendix D. Renormalization and Residual Background	88
VITA	90

LIST OF TABLES

TABLE		PAGE
3-1.	Numerical comparison of the two methods	29
4-1.	Selected measurements of the ^{235}U neutron cross sections .	35
5-1.	2200 m/s value of the cross sections at 300 K (b)	43
5-2.	Comparison of ^{235}U integrated cross sections $\int \sigma dE$ (b eV)	52
5-3.	Comparison of average fission cross sections (b)	56
5-4.	Comparison of fission and capture resonance integrals (b) .	61
5-5.	Average value of observed ^{235}U resonance parameters (eV)	68
5-6.	Comparison of fission and capture selfshielding factors . . .	70
C-1.	Evaluated Reich-Moore resonance parameters	85
C-2.	Adler-Adler resonance parameters	86
C-3.	Multipole momentum space resonance parameters	87
D-1.	Renormalization and residual background	88

LIST OF FIGURES

FIGURE	PAGE
3-1. ^{235}U fission cross section broadened to 300 K and calculated by the two methods	30
5-1. Comparison of the total cross-section data of Spencer et al., fission cross-section data of Gwin et al., and Wagemans et al. with calculations using the resonance parameters	42
5-2. Comparison of the transmission data of Harvey et al. with calculations using the resonance parameters. The two upper curves have been displaced upward by 0.5 for clarity	44
5-3. Comparison of the transmission data of Harvey et al. with calculations using the resonance parameters. The two upper curves have been displaced upward by 0.5 for clarity	45
5-4. Comparison of the transmission data of Harvey et al. with calculations using the resonance parameters. The two upper curves have been displaced upward by 0.5 for clarity	46
5-5. Comparison of the transmission data of Harvey et al. with calculations using the resonance parameters	47
5-6. Comparison of the fission cross-section data of Schrack and of Gwin et al. with calculations using the resonance parameters	48
5-7. Comparison of the fission cross-section data of Blons and of Weston and Todd with calculations using the resonance parameters	49
5-8. Comparison of the fission cross-section data of Blons and of Weston and Todd with calculations using the resonance parameters	50
5-9. Comparison of the fission cross-section data of Blons and of Weston and Todd with calculations using the resonance parameters	51
5-10. Comparison of the spin separated fission cross-section data of Moore et al. with calculations using the resonance parameters	53
5-11. Comparison of the spin separated fission cross-section data of Moore et al. with calculations using the resonance parameters	54

FIGURE	PAGE
5-12. Comparison of the capture cross-section data of de Saussure et al. compared with calculations using the resonance parameters . . .	55
5-13. Comparison of the total cross section of Harvey et al., fission cross section of Weston and Todd, and capture cross section of de Saussure et al. with calculations using the resonance parameters . . .	57
5-14. Comparison of the total cross section of Harvey et al., fission cross section of Weston and Todd, and capture cross section of de Saussure et al. with calculations using the resonance parameters . . .	58
5-15. Comparison of the total cross section of Harvey et al., fission cross section of Weston and Todd, and capture cross section of de Saussure et al. with calculations using the resonance parameters . . .	59
5-16. Comparison of the total cross section of Harvey et al., fission cross section of Weston and Todd, and capture cross section of de Saussure et al. with calculations using the resonance parameters . . .	60
5-17. Reduced neutron-width distributions compared to Porter-Thomas distributions	63
5-18. Fission-width distributions compared to χ^2 distribution with two degrees of freedom	64
5-19. Nearest neighbor-spacing distributions compared to Wigner distributions	65
5-20. Cumulative number of energy levels vs. energy. The steps of the histograms can not be seen in that scale	67
D-1. Residual background on the fission cross-section data of Blons .	89

ABSTRACT

Neutron cross sections of fissile nuclei are of considerable interest for the understanding of parameters such as resonance absorption, resonance escape probability, resonance self-shielding, and the dependence of the reactivity on temperature.

In the present study, new techniques for the evaluation of the ^{235}U neutron cross sections are described. The Reich-Moore formalism of the Bayesian computer code SAMMY was used to perform consistent R -matrix multilevel analyses of the selected neutron cross-section data. The Δ_3 -statistics of Dyson and Mehta, along with high-resolution data and the spin-separated fission cross-section data, have provided the possibility of developing a new methodology for the analysis and evaluation of neutron-nucleus cross sections. The result of the analysis consists of a set of resonance parameters which describe the ^{235}U neutron cross sections up to 500 eV.

The set of resonance parameters obtained through a R -matrix analysis are expected to satisfy statistical properties which lead to information on the nuclear structure. The resonance parameters were tested and showed good agreement with the theory.

It is expected that the parametrization of the ^{235}U neutron cross sections obtained in this dissertation represents the current state of art in data as well as in theory and, therefore, can be of direct use in reactor calculations.

CHAPTER I

INTRODUCTION

High-resolution neutron cross-section measurements taken in the past 20 years, as well as the development of new techniques for the treatment of experimental data, have created a strong incentive for the reevaluation of several materials in the nuclear data libraries. Furthermore, the increasing need of very accurate nuclear data for reactor design and calculations has required good representation of experimental data to guarantee consistency between theoretical models and experimental results.

Nuclear data for reactor calculations are, in general, based on the total, fission, capture, and scattering cross sections of the reaction neutron-nucleus.

From a technical point of view, knowledge of the resonance parameters and average cross sections is of interest for the design and development of nuclear reactors since the resonance structure of the neutron cross sections determines the values and the energy dependence of reactor properties such as resonance absorption, resonance escape probability, resonance self-shielding factors, and the dependence of the reactivity on temperature (Doppler coefficient).

In particular, due to the importance of fissile materials in nuclear reactors, the neutron cross sections of fissile nuclei have continued to remain a source of considerable interest to understand reactor parameters.

The purpose of this work is to develop new techniques which, when combined with present methods, will lead to an updated, meaningful representation of neutron-induced cross sections for fissile isotopes.

The study of neutron-nucleus interactions is a remarkable example of the direct application of quantum physics to a highly technical and industrial task such as the

design of a nuclear power plant. Specifically, this work will describe the procedures, method of analysis, and selection of experimental data which are needed to obtain by neutron spectroscopy measurements and theory a consistent set of evaluated ^{235}U neutron cross sections for nuclear reactor core design. It should be noted that ^{235}U is not only an important fuel for commercial reactors using slightly enriched uranium as initial fuel and for research reactors using highly enriched uranium, but the cross section of ^{235}U is often used as a standard by which other cross sections are measured.

1.0 BACKGROUND

Various steps are required before measured data are available in a suitable form for reactor design and calculations. Evaluated data from several evaluation centers in the world are submitted to nuclear data libraries which test and prepare the data for application to nuclear technology.

The most important nuclear data libraries are the United States Nuclear Data File (ENDF), the United Kingdom Nuclear Data Library (UKNDL), the German files (KEDAK), the Soviet Union files (SOKRATOR), the Joint European Files (JEF), and the Japan Evaluated Nuclear Data Library (JENDL). These nuclear data files are available from the USA National Nuclear Data Center.¹

There are two libraries associated with the ENDF system; namely, the ENDF/A and the ENDF/B libraries. The ENDF/A is a collection of evaluated data from different evaluation centers. The Cross Section Evaluation Working Group (CSEWG) recommends the selected data which are included in the ENDF/B libraries in a format suitable for reactor design and calculations. The present version of ENDF/B is ENDF/B-VI and is still under review. In ENDF/B,

neutron cross sections may be represented by specifying actual resonance parameters (resolved resonance region), or specifying statistical distribution of parameters (unresolved resonance region), or the cross sections may be given at discrete energy points with a specified interpolation rule (pointwise or FILE 3 representation). The cross sections may also be given as sums of contributions from these representations.

The cross-section representations are reconstructed from the resonance parameters according to a formalism specified by the evaluator. Four cross-section formalisms are permitted in the ENDF files for the resolved energy region. They are the single-level Breit-Wigner (SLBW), the multilevel Breit-Wigner (MLBW), the Adler-Adler (AA), and the Reich-Moore (RM) formalisms.

The evaluation of the ^{235}U neutron cross sections in the present work was performed using the Reich-Moore formalism up to 500 eV. The set of resonance parameters obtained by the Reich-Moore formalism were also converted to equivalent Adler-Adler and multipole representations.

1.1 NEED FOR THE PRESENT WORK

A parametric representation of the neutron cross sections of fissile elements cannot be given by a formalism that does not account for the asymmetries in the resonances of the reaction cross section. Such asymmetries, which are due to the level-level interference in the fission channels, can only be described by a multilevel formalism.

The neutron cross-section representation of ^{235}U in ENDF/B-V for the resolved energy region is based on an evaluation performed in 1970 for ENDF/B-III which utilized the single-level Breit-Wigner formalism. Since the ^{235}U levels are closely spaced, such a formalism is inadequate to describe correctly the level-level

interference and, hence, is not appropriate to describe the ^{235}U neutron cross sections.

The palliation used in the ENDF files to overcome the deficiency of the Breit-Wigner formalism was to add a “smooth contribution” to the cross section. The “smooth file” (FILE 3 contribution), consisting of more than 1300 points, contains the difference between the calculated Breit-Wigner cross sections and the experimental cross sections. The main disadvantage is that this approach is not based on a meaningful reaction theory. Also, information on the level-spin is not included; all levels are assigned a fictitious value. Finally, the parametric representation extends up to 82 eV only.

It is obvious that the ENDF/B-III evaluation has not included the results of several high quality measurements done in the past 20 years. It is, therefore, highly desirable to re-evaluate the ^{235}U neutron cross sections to better represent the current state of art in data as well as in theory.

1.2 OBJECTIVES

The purpose of this work is to develop a new evaluation of the ^{235}U neutron cross sections. The choice of experimental data and the criteria used in selecting the experimental data entering the analysis will be discussed. We will also outline the method of analysis and the representation of the data by showing graphical and tabular comparisons of the cross sections obtained from the theoretical calculations using resonance parameters with several experimental and evaluated data sets. Another objective is to test the validity of the unresolved resonance parameter representation of the cross sections by comparing self-shielding calculations in the 82–500 eV region, where ENDF/B-V cross sections are defined by unresolved

(statistical) resonance parameters and the present analysis provides a resolved resonance representation.

The pertinent steps of the evaluation consist of the selection of the experimental data and method of analysis. Most of the experimental data available on the Cross-Section Information Standard Retrieval System (CSISRS)² or listed in The Computer Index of Neutron DATA (CINDA)³ were examined for possible inclusion in the analysis. Detailed information on the experimental conditions and the systematic uncertainties of the experimental data was essential for the choice of data.

The main data included in the analysis came from recent measurements performed at the Oak Ridge Electron Linear Accelerator (ORELA).⁴ These data were chosen because of the high resolution and because detailed descriptions of the experimental conditions were readily accessible. The data were transmission (total cross-section), fission cross-section, and capture cross-section measurements.

The data analysis was performed using the computer code SAMMY.⁵ The computer code SAMMY accommodates the reduced R -matrix Reich-Moore formalism which is appropriate to treat the neutron cross sections of fissile elements. The fitting procedure of SAMMY is based on the Bayes' method and allows the successive incorporation of new data.

1.3 ORGANIZATION OF THE DISSERTATION

The material in this dissertation is organized as follows. Chapter I presents a general overview of the neutron cross-section evaluation process and outlines the approach pursued. The theoretical background necessary for the formulation of the various neutron cross-section formalisms used in the evaluation process and for the study of the statistical properties of the resonance parameters is given in

Chapter II. The Doppler broadening and instrumental effects, such as resolution broadening, normalization, and background corrections, are discussed in Chapter III. The experimental data in the analysis are described in Chapter IV. Chapter V describes the methods employed in the analysis and provides graphical and tabular comparisons between the data and the corresponding theoretical calculations. The conclusions are presented in Chapter VI. Some analytical details concerning nuclear reactor theory are given in four appendices.

1.4 ACCOMPLISHMENTS

For the first time, a set of neutron resonance parameters for the representation of ^{235}U neutron cross sections have been obtained for a wide neutron energy range which extends the resolved resonance region from its present limit of 82 eV up to 500 eV. This unprecedented result provided the possibility of performing a thorough analysis of the unresolved resonance methodology used for the calculation of a self-shielded group of cross sections for reactor core design.

New procedures were developed to facilitate the process of neutron cross-section resonance analysis. These procedures include the methodical evaluation of cross-section data to select the best available measurements, the development of a procedure for Doppler-broadening neutron resonances which have been incorporated in the ORNL Bayesian program SAMMY, and the use of Dyson's Δ_3 -statistics for resonance spin assignments.

The problem of representing neutron cross sections in the resolved resonance region at the core of the ENDF/B format and procedure prescriptions for nuclear reactor designers has been approached in an ample and original manner. The conversion of the R -matrix parameters obtained in this work into Kapur-Peierls resonance parameters and the use of multipole expansions in the momentum space

have provided the necessary data for the use of alternative cross-section representations such as the Adler-Adler neutron cross-section formulation.

The present set of ^{235}U neutron resonance parameters have made a precise and extensive study of the statistical properties of the ^{236}U nuclear Hamiltonian (i.e., energy eigenvalues and resonance width) possible which, until now, was hindered by the comparatively small amount of statistical samples available.

It is believed that the contents of this dissertation will have an important impact on the study of nuclear reaction theory. Furthermore, the results of this work have been accepted for inclusion in the ENDF/B Files and will be of direct use in nuclear reactor design.

CHAPTER II

RESONANCE THEORY

Resonance theory deals with the description of nucleon-nucleus interactions and aims at the prediction of the experimental structure of the cross sections. Resonance theory is basically an interaction model which treats the nucleus as a black box, whereas nuclear models are concerned with the description of nuclear properties based on models of the nuclear forces. Any theoretical method of calculating the neutron-nucleus interactions or nuclear properties cannot fully describe the nuclear effects inside the nucleus because of the complexity of the nucleus and because the nuclear forces, acting within the nucleus, are not known in detail. Quantities related to internal properties of the nucleus are taken, in this nuclear theory, as parameters which can be determined by examining the experimental results.

The general R -matrix theory, introduced by Wigner and Eisenbud⁶ in 1947, is a powerful nuclear interaction model. Despite the generality of the theory, it does not require information on the internal structure of the nucleus; instead, the unknown internal properties, appearing as elements in the R -matrix, are treated as parameters and can be determined by examining the measured cross sections.

Throughout the present work, the interaction models which are used to describe the neutron-nucleus cross sections that we will be dealing with, are specializations of the general R -matrix theory. The practical aspects of the general R -matrix theory as well as the relationship between the collision matrix and the R -matrix will be presented. Also, the difficulties which one encounters in evaluating the cross sections by the direct use of the general R -matrix theory will be

pointed out. The approximations needed for obtaining the simplified R -matrix models will also be addressed.

2.0 OVERVIEW OF R -MATRIX THEORY

The general R -Matrix theory has been extensively described by Lane and Thomas.⁷ An overview is presented here as an introduction to the resonance formalisms which will be described later.

To understand the basic points of the general R -matrix theory, we will consider a simple case of neutron collision in which the spin dependence of the constituents of the interactions is neglected. Although the mathematics involved in this special case is over-simplified, it nevertheless contains the essential elements of the general theory.

As mentioned before, the nuclear potential inside the nucleus is not known, and, therefore, the behavior of the wave function in the internal region of the nucleus cannot be calculated directly from the Schrödinger equation. The R -matrix analysis of expands the inner wave function of angular momentum l as a linear combination of the eigenfunctions of the energy levels in the compound nucleus. Mathematically speaking, if $\phi_l(E, r)$ is the inner wave function at any energy E and $\phi_l(E_\lambda, r)$ is the eigenfunction at the energy eigenvalue E_λ the relation becomes

$$\phi_l(E, r) = \sum_{\lambda} A_{l\lambda} \phi_l(E_\lambda, r) . \quad (2-1)$$

Both $\phi_l(E, r)$ and $\phi_l(E_\lambda, r)$ are solutions of the radial Schrödinger equations in the internal region given by

$$\left\{ \frac{d^2}{dr^2} + \frac{2m}{\hbar^2} \left[E - V(r) - \frac{l(l+1)\hbar^2}{2mr^2} \right] \right\} \phi_l(E, r) = 0 \quad (2-2)$$

and

$$\left\{ \frac{d^2}{dr^2} + \frac{2m}{\hbar^2} \left[E_\lambda - V(r) - \frac{l(l+1)\hbar^2}{2mr^2} \right] \right\} \phi_l(E_\lambda, r) = 0 . \quad (2-3)$$

The finite condition at $r = 0$ implies that both functions vanish at that point. In addition, the logarithmic derivative of the eigenfunction at the nuclear surface, say $r = a$, is taken to be constant so that

$$\left[\frac{d\phi_l(E_\lambda, r)}{dr} \right]_{r=a} = a^{-1} B_l \phi_l(E_\lambda, a) , \quad (2-4)$$

where B_l is an arbitrary boundary constant.

Since we are dealing with eigenfunctions of a real Hamiltonian, they are orthogonal. Assuming that they are also normalized, we have

$$\int_0^a \phi_l(E_\lambda, r) \phi_l(E_{\lambda'}, r) dr = \delta_{\lambda\lambda'} . \quad (2-5)$$

From Eq. (2-1) and the orthogonality condition, we find the coefficient $A_{l\lambda}$,

$$A_{l\lambda} = \int_0^a \phi_l(E_\lambda, r) \phi_l(E, r) dr . \quad (2-6)$$

To proceed to the construction of the R -matrix, Eq. (2-2) is multiplied by $\phi_l(E_\lambda, r)$ and Eq. (2-3) is multiplied by $\phi_l(E, r)$. Subtracting and integrating the result over the range from 0 to a and from Eq. (2-6) the expression obtained for the coefficient $A_{l\lambda}$ is

$$A_{l\lambda} = \frac{\hbar^2}{2ma} (E_\lambda - E)^{-1} \left[\phi_l(E_\lambda, r) \frac{d\phi_l(E, r)}{dr} - \phi_l(E, r) \frac{d\phi_l(E_\lambda, r)}{dr} \right]_{r=a} . \quad (2-7)$$

Inserting $A_{l\lambda}$ into Eq. (2-1) for $r = a$ at the surface of the nucleus and using Eq. (2-4), the wave function is given by

$$\phi_l(E, a) = \frac{\hbar^2}{2ma} \sum_\lambda \left[\frac{\phi_l(E_\lambda, a) \phi_l(E_\lambda, a)}{E_\lambda - E} \right] \left[r \frac{d\phi_l(E, r)}{dr} - B_l \phi_l(E, r) \right]_{r=a} . \quad (2-8)$$

Equation (2-8) relates the value of the inner wave function with its derivative at the surface of the nucleus. The R matrix is defined as follows

$$R_l = \frac{\hbar^2}{2ma} \sum_{\lambda} \frac{\phi_l(E_{\lambda}, a) \phi_l'(E_{\lambda}, a)}{E_{\lambda} - E} \quad (2-9)$$

or

$$R_l = \sum_{\lambda} \frac{\gamma_{\lambda l} \gamma_{\lambda l}}{E_{\lambda} - E} , \quad (2-10)$$

where $\gamma_{\lambda l}$, the reduced width amplitude for the level λ and angular momentum l , is defined as

$$\gamma_{\lambda l} = \sqrt{\frac{\hbar^2}{2ma}} \phi_l(E_{\lambda}, a) . \quad (2-11)$$

The reduced width amplitude depends on the value of the inner wave function at the nuclear surface. Both E_{λ} and $\gamma_{\lambda l}$ are the unknown parameters of the R matrix which can be evaluated by examining the measured cross sections.

The generalization of Eq. (2-10) is obtained by including the neutron-nucleus spin dependence and several possibilities in which the reaction process can occur. The concept of channel is introduced to designate a possible pair of nucleus and particles and the spin of the particles. The channel containing the initial state is called the entrance channel (c), whereas the channel containing the final state is the exit channel or final channel (c'). The elements of the R matrix in the general case are given by

$$R_{cc'} = \sum_{\lambda} \frac{\gamma_{\lambda c} \gamma_{\lambda c'}}{E_{\lambda} - E} , \quad (2-12)$$

where the reduced width amplitude is given by

$$\gamma_{\lambda c} = \sqrt{\frac{\hbar^2}{2m_c a_c}} \phi_c(E_{\lambda}, a_c) . \quad (2-13)$$

The next objective is to relate the R -matrix with the cross-section formalism so the cross sections can be computed once the elements of the R -matrix are known.

The general expressions for the neutron-nucleus cross sections are based on the collision matrix, also known as U -matrix, whose elements are unknown. The nice feature of the R -matrix is that the unknown elements of the U -matrix can be expressed by the elements of the R -matrix. To derive the relationship between the U and R matrices, we will proceed by analyzing a simple case of spinless neutral particles.

The total wave function in the region outside the nuclear potential can be expressed as a linear combination of the incoming and outgoing wave functions. If $\phi_l^{\text{in}}(r)$ and $\phi_l^{\text{out}}(r)$ are, respectively, the incoming and outgoing wave functions for a free particle, the solution of the radial Schrödinger equation can be written as

$$\phi_l(r) = C_l[\phi_l^{\text{in}}(r) - U_l\phi_l^{\text{out}}(r)] \quad \text{for } r \geq a \quad , \quad (2 - 14)$$

where C_l is a normalization constant.

The presence of the U -matrix in Eq. (2-14) (in this case, a matrix of one element) indicates that the amplitudes of the incoming and outgoing wave function are different unless $|U_l| = 1$ corresponds to pure elastic scattering which means that no reaction has occurred.

The Schrödinger equation for $\phi_l^{\text{in}}(r)$ and $\phi_l^{\text{out}}(r)$ is the same as Eq. (2-2) with $V(r) = 0$ since there is no potential outside the nucleus. The solution is a combination of the spherical Bessel and Neumann functions

$$\phi_l^{\text{in}}(r) = kr [n_l(kr) + ij_l(kr)] \quad , \quad (2 - 15)$$

and

$$\phi_l^{\text{out}}(r) = kr [n_l(kr) - ij_l(kr)] \quad , \quad (2 - 16)$$

where $i = \sqrt{-1}$.

The relation between the U and the R -matrices is obtained by noting that Eq. (2-8) can be written as

$$\phi_l(E, a) = \left[r \frac{d\phi_l(E, r)}{dr} - B_l \phi_l(E, r) \right]_{r=a} R_l . \quad (2-17)$$

Equation (2-17), when combined with Eq. (2-14), provides the relation between the R and U -matrices as

$$U_l = \left(\frac{\phi_l^{\text{in}}}{\phi_l^{\text{out}}} \right)_{r=a} \frac{1 - \left[\left(\frac{r}{\phi_l^{\text{in}}} \frac{d\phi_l^{\text{in}}}{dr} \right)_{r=a} - B_l \right] R_l}{1 - \left[\left(\frac{r}{\phi_l^{\text{out}}} \frac{d\phi_l^{\text{out}}}{dr} \right)_{r=a} - B_l \right] R_l} . \quad (2-18)$$

We define the logarithmic derivative as

$$L_l = \left(\frac{r}{\phi_l^{\text{out}}} \frac{d\phi_l^{\text{out}}}{dr} \right)_{r=a} . \quad (2-19)$$

Since from Eqs. (2-15) and (2-16), ϕ_l^{in} and ϕ_l^{out} are complex conjugate,

$$L_l^* = \left(\frac{r}{\phi_l^{\text{in}}} \frac{d\phi_l^{\text{in}}}{dr} \right)_{r=a} . \quad (2-20)$$

Equation (2-18) becomes

$$U_l = \left(\frac{\phi_l^{\text{in}}}{\phi_l^{\text{out}}} \right)_{r=a} \frac{1 - (L_l^* - B_l) R_l}{1 - (L_l - B_l) R_l} . \quad (2-21)$$

Equation (2-21), which allows the prediction of the neutron-nucleus cross sections, represents the desired relationship between the collision matrix U and the matrix R . From the basic quantum mechanics theory,⁸ the cross sections for the neutron-nucleus interaction can be given as a function of the matrix U as

(a) elastic-scattering cross section

$$\sigma_n = \pi \lambda^2 \sum_l (2l+1) |1 - U_l|^2 , \quad (2-22)$$

(b) reaction cross section

$$\sigma_r = \pi \lambda^2 \sum_l (2l + 1) (1 - |U_l|^2) , \quad (2-23)$$

(c) total cross section

$$\sigma_t = 2\pi \lambda^2 \sum_l (2l + 1) (1 - \text{Re} |U_l|) , \quad (2-24)$$

where λ is the neutron reduced wavelength given by

$$\lambda = \frac{\hbar}{\sqrt{2mE}} . \quad (2-25)$$

The representation of the neutron cross sections will depend on the reduced width amplitudes $\gamma_{\lambda c}$'s as well as the E_λ 's which are the unknown parameters of Eq. (2-21). Those parameters, as mentioned before, are obtained by fitting the experimental cross sections.

The general relation between the matrices U and R , which are similar to Eq. (2-21) with each term converted to matrix form, is

$$\mathbf{U} = \rho^{1/2} \Phi_{\text{out}}^{-1} [\mathbf{I} - \mathbf{R}(\mathbf{L} - \mathbf{B})]^{-1} [\mathbf{I} - \mathbf{R}(\bar{\mathbf{L}} - \mathbf{B})] \Phi_{\text{in}} \rho^{-1/2} . \quad (2-26)$$

All the matrices in Eq. (2-26) are diagonal except the \mathbf{R} matrix in which the elements are the unknown quantities. The matrix $\rho^{1/2}$ contains the elements $(k_c a_c)^{1/2}$.

Since no approximation was used in deriving Eq. (2-26) it represents an exact expression relating the matrices \mathbf{U} and \mathbf{R} . Unfortunately, Eq. (2-26) cannot be used directly for the prediction of the neutron-nucleus cross sections because it would require the knowledge of the unknown elements of the matrix \mathbf{R} and the inversion of matrices of large sizes. Therefore, several approximations of the R -matrix theory have been introduced which lead to various cross-section formalisms.

Another presentation of Eq. (2-26) may be obtained by introducing the following definitions

$$\mathbf{L}_0 = \mathbf{S}_0 - i\mathbf{P} , \quad (2-27)$$

$$\mathbf{L}_0 = \mathbf{L} - \mathbf{B} , \quad (2-28)$$

$$\mathbf{S}_0 = \mathbf{S} - \mathbf{B} , \quad (2-29)$$

where \mathbf{S} and \mathbf{P} are matrices which contain the shift and penetration factors, respectively.

The penetration factors can be written as $\mathbf{P} = \rho(\phi_{\text{in}}\phi_{\text{out}})^{-1}$, and Eq. (2-26) becomes

$$\mathbf{U} = \mathbf{\Omega} \left[\mathbf{I} + 2i\mathbf{P}^{1/2} \left(\mathbf{I} - \mathbf{R}\mathbf{L}_0 \right)^{-1} \mathbf{R}\mathbf{P}^{1/2} \right] \mathbf{\Omega} , \quad (2-30)$$

with $\mathbf{\Omega} = \phi_{\text{in}}^{1/2} \phi_{\text{out}}^{-1/2}$.

The channel matrix $(\mathbf{I} - \mathbf{R}\mathbf{L}_0)^{-1} \mathbf{R}$ may be related to the level matrix $A_{\mu\lambda}$ as follows:

$$(\mathbf{I} - \mathbf{R}\mathbf{L}_0)^{-1} \mathbf{R} = \sum_{\mu\lambda} (\gamma_\mu \times \gamma_\lambda) A_{\mu\lambda} , \quad (2-31)$$

where μ and λ refer to energy levels in the compound nucleus. The level matrix $A_{\mu\lambda}$ satisfies the equation

$$A_{\lambda\nu}(E_\lambda - E) - \sum_{\mu} (L_0 \gamma_\lambda \cdot \gamma_\mu) A_{\mu\nu} = \delta_{\lambda\nu} . \quad (2-32)$$

Details of the derivation of the equations above are given in Appendix A.

The collision matrix is related to the level matrix as

$$\mathbf{U} = \mathbf{\Omega} \left[\mathbf{I} + 2i\mathbf{P}^{1/2} \left(\sum_{\mu\nu} (\gamma_\mu \times \gamma_\nu) A_{\mu\nu} \right) \mathbf{P}^{1/2} \right] \mathbf{\Omega} . \quad (2-33)$$

The elements of the collision matrix for an entrance and exit channel (c) and (c'), respectively, are given as

$$U_{cc'} = \Omega_c \left(\delta_{cc'} + i \sum_{\mu\lambda} \Gamma_{\mu c}^{1/2} A_{\mu\lambda} \Gamma_{\lambda c'}^{1/2} \right) \Omega_{c'} , \quad (2-34)$$

where

$$\Gamma_{\mu c}^{1/2} = \gamma_{\mu c}(2P_c)^{1/2} \quad (2-35)$$

is the level width and, from Eq. (2-32)

$$A_{\mu\lambda}^{-1} = (E_\lambda - E)\delta_{\mu\lambda} - \sum_c \gamma_{\mu c} L_{0c} \gamma_{\lambda c} \quad (2-36)$$

Either Eq. (2-26) or Eq. (2-33) will provide the elements of the collision matrix. It should be remembered that no approximation has been introduced in the formal derivation of the collision matrix yet.

2.1 REDUCED R-MATRIX FORMALISM (REICH-MOORE FORMALISM)

The approach introduced by Reich and Moore⁹ for treating the neutron-nucleus cross sections consists of eliminating the off-diagonal contribution of the photon channels. The approximation is justified since the reduced width amplitudes have random signs, exhibit random size variation,¹⁰ and the sum $\sum_{c \in \gamma} \gamma_{\mu c} \gamma_{\lambda c}$ is very small if $\mu \neq \lambda$ due to the large number of gamma channels. Such an assumption reduces considerably the problem of inverting a large matrix and, therefore, is suitable to deal with cases in which a few channels and many levels are present. The fission process proceeds through a small number of channels,¹¹ and the Reich-Moore formalism is convenient to describe the neutron-nucleus cross section of fissile elements.

The elimination of the radiation-capture channels in the Reich-Moore approach is obtained by partitioning the R -matrix into a 2-by-2 matrix in which each element is a matrix. The contribution of the radiative-capture channels is isolated from

the neutron and fission channels. Assuming one neutron channel, $m - 1$ fission channel, and n radiative-capture channel the partitioning is given by

$$\mathbf{R} = \begin{pmatrix} \mathbf{R}_{m \times m} & \mathbf{R}_{m \times n} \\ \mathbf{R}_{n \times m} & \mathbf{R}_{n \times n} \end{pmatrix}, \quad (2-37)$$

where the matrix $\mathbf{R}_{m \times m}$ contains the neutron and fission channel contributions and the radiative-capture contributions are included in the matrix $\mathbf{R}_{n \times n}$.

The next step consists of substituting Eq. (2-37) into $(\mathbf{I} - \mathbf{R}\mathbf{L}_0)^{-1}$ of the \mathbf{U} matrix given by Eq. (2-30) and inverting the resulting 2-by-2 block matrix. The inverted 2-by-2 matrix has elements given by $(\mathbf{I} - \mathbf{R}\mathbf{L}_0)_{n \times n}^{-1}$ which contain only the radiative-capture contributions. The evaluation of $(\mathbf{I} - \mathbf{R}\mathbf{L}_0)_{n \times n}^{-1}$ is performed using the relation

$$(\mathbf{I} - \mathbf{R}\mathbf{L}_0)_{n \times n}^{-1} = \mathbf{1} + \sum_{\mu\lambda} (\gamma_\mu \times \gamma_\lambda) \mathbf{A}_{\mu\lambda}. \quad (2-38)$$

In the level matrix $\mathbf{A}_{\mu\lambda}$, only the channels corresponding to the radiative-capture channels are considered, and from Eq. (2-36) it gives

$$A_{\mu\lambda}^{-1} = (E_\lambda - E) \delta_{\mu\lambda} - \sum_{c \in \gamma} \gamma_{\mu c} L_{0c} \gamma_{\lambda c}. \quad (2-39)$$

The Reich-Moore approximation consists of writing the summation correspondent to the gamma channel as follows:

$$\sum_{c \in \gamma} \gamma_{\mu c} L_{0c} \gamma_{\lambda c} = \sum_{c \in \gamma} L_{0c} \gamma_{\mu c}^2 \delta_{\mu\lambda}. \quad (2-40)$$

Since $L_{0c} = S_{0c} + iP_c$, Eq. (2-40) becomes

$$\sum_{c \in \gamma} \gamma_{\mu c} L_{0c} \gamma_{\lambda c} = \Delta_{\lambda\gamma} + \frac{i}{2} \Gamma_{\lambda\gamma}, \quad (2-41)$$

where

$$\Delta_{\lambda\gamma} = - \sum_{c \in \gamma} S_{0c} \gamma_{\lambda c}^2 \quad (2-42)$$

and

$$\Gamma_{\lambda\gamma} = \sum_{c \in \gamma} \Gamma_{\lambda c} . \quad (2-43)$$

The level matrix becomes

$$A_{\mu\lambda} = \frac{\delta_{\mu\lambda}}{E'_\lambda - E - \frac{i}{2} \Gamma_{\lambda\gamma}} , \quad (2-44)$$

with

$$E'_\lambda = E_\lambda + \Delta_{\lambda\gamma} . \quad (2-45)$$

In the equations above, $\Delta_{\lambda\gamma}$ is called the level shift caused by photon channels and $\Gamma_{\lambda\gamma}$ is the radiation width.

Substituting Eq. (2-44) into Eq. (2-38) gives

$$(\mathbf{I} - \mathbf{R}\mathbf{L}_0)_{n \times n}^{-1} = \mathbf{1} + \sum_{\lambda} \frac{\gamma_{\lambda} \times \gamma_{\lambda}}{E'_\lambda - E - \frac{i}{2} \Gamma_{\lambda\gamma}} . \quad (2-46)$$

The remaining portions of $(\mathbf{I} - \mathbf{R}\mathbf{L}_0)^{-1}$ are matrices containing the neutron and fission channels. The Reich-Moore assumption leads to a collision matrix having the same form as that given in Eq. (2-30) except the R -matrix is modified as

$$\mathbf{R} = \sum_{\lambda} \frac{\gamma_{\lambda} \times \gamma_{\lambda}}{E_{\lambda} - E - \frac{i}{2} \Gamma_{\lambda\gamma}} . \quad (2-47)$$

The elements of the collision matrix can be expressed as

$$U_{cc'} = \Omega_c \left[2(I - K)_{cc'}^{-1} - \delta_{cc'} \right] \Omega_{c'} , \quad (2-48)$$

where

$$(I - K)_{cc'} = \delta_{cc'} - \frac{i}{2} \sum_{\lambda} \frac{\Gamma_{\lambda c}^{1/2} \Gamma_{\lambda c'}^{1/2}}{E'_\lambda - E - \frac{i}{2} \Gamma_{\lambda\gamma}} . \quad (2-49)$$

2.2 ADLER-ADLER FORMALISM

Another approximation to the level matrix is that introduced by Adler and Adler.¹² The technique developed by Adler and Adler consists of diagonalizing the inverse level matrix by an orthogonal transformation as follows:

$$\mathbf{D} = \mathbf{S}^{-1} \mathbf{A} \mathbf{S} . \quad (2-50)$$

The elements of the level matrix under the transformation given by the Eq. (2-50) are written as

$$A_{\mu\lambda} = \sum_{\nu} \frac{S_{\mu\nu} S_{\lambda\nu}}{d_{\nu} - E} . \quad (2-51)$$

Introducing the Adler-Adler approximation in the collision matrix given by Eq. (2-34) we have

$$U_{cc'} = \Omega_c \left[\delta_{cc'} + \sum_{\nu} \frac{r_{\nu cc'}}{d_{\nu} - E} \right] \Omega_{c'} , \quad (2-52)$$

with

$$r_{\nu cc'} = \sum_{\mu\lambda} \Gamma_{\mu c}^{1/2} S_{\mu\nu} S_{\lambda\nu} \Gamma_{\lambda c'}^{1/2} . \quad (2-53)$$

The parameters d_{ν} and $r_{\nu cc'}$ are complex, in contrast with the parameters of the Reich-Moore formalism which are real. Because of the energy dependence of the reduced neutron width, the diagonalization of the level matrix would be required at every energy point in order to preserve the rigor of the Adler-Adler formalism. However, for low-energy *s*-wave neutrons, the neutron width is very small compared to the gamma and fission widths, and its energy dependence can be neglected. In this case, the Adler-Adler formalism is very efficient to represent the neutron-nucleus cross sections, although one should be aware of this limitation which could otherwise lead to a misrepresentation of the cross sections.

Since the Adler-Adler formalism lends itself easily to the generation of Doppler broadened cross sections, it has been included as an option for the representation of low-energy neutron cross sections in the ENDF/B format and procedures.

A general procedure to convert Reich-Moore type parameters into an equivalent set of Adler-Adler parameters was developed by de Saussure and Perez.¹³ Their approach consisted of writing the Reich-Moore transmission probabilities ρ_{nn} and ρ_{nc} (see Appendix B) as the ratios of polynomials in energies which, subsequently, can be expressed in terms of partial fraction expansions, matching the Adler-Adler cross section formulation, i.e:

$$\frac{1}{\sqrt{E}}\rho_{nn} = \frac{P_n^{(N-1)}(E)}{P^{(N)}(E)} = \sum_{\lambda=1}^N \frac{r_{\lambda n}}{d_{\lambda} - E} , \quad (2-54)$$

and

$$\frac{1}{\sqrt{E}}\rho_{nc} = \frac{|P_c^{(N-1)}(E)|^2}{|P^{(N)}(E)|^2} = \sum_{\lambda=1}^N \left[\frac{r_{\lambda c}}{d_{\lambda} - E} + \frac{r_{\lambda c}^*}{d_{\lambda}^* - E} \right] \quad c \neq n , \quad (2-55)$$

where

$$P^{(N)} = Q\Delta , \quad (2-56)$$

$$P_n^{(N-1)} = Q \frac{\Delta - m_{nn}}{\sqrt{E}} , \quad (2-57)$$

$$|P_c^{(N-1)}|^2 = \frac{|Q \cdot m_{nc}|^2}{\sqrt{E}} , \quad (2-58)$$

and

$$Q = \prod_{\lambda} (E_{\lambda} - E - \frac{i}{2}\Gamma_{\lambda\gamma}) . \quad (2-59)$$

Equations (2-54) and (2-55) have poles $d_{\lambda} = \mu_{\lambda} - i\nu_{\lambda}$ which are roots of the equation

$$P^{(N)}(E) = Q \Delta = 0 \quad (2-60)$$

and are identifiable as the parameters of the Adler-Adler formalism.

A detailed account of the construction of neutron cross sections from Reich-Moore and Adler-Adler resonance parameters is given in Appendix B.

2.3 EXPANSION OF THE COLLISION MATRIX IN MOMENTUM SPACE

Based on the rationale that the collision matrix must be single-valued and mesomorphic in the momentum space and the fact that any function that satisfies such a condition must be a rational function with simple poles, one can rigorously express the quantities ρ_{nn} and ρ_{nc} in terms of pole expansion in momentum space. For s -wave, one has

$$\frac{1}{\sqrt{E}}\rho_{nn} = \sum_{\lambda=1}^{2N} \frac{R_{\lambda n}}{D_{\lambda} - \sqrt{E}} , \quad (2-61)$$

and

$$\frac{1}{\sqrt{E}}\rho_{nc} = \sum_{\lambda=1}^{2N} \left[\frac{R_{\lambda n}}{D_{\lambda} - \sqrt{E}} + cc \right] , \quad (2-62)$$

where the residues $R_{\lambda n}$ and poles D_{λ} are now strictly energy independent. Hence, the expansion in momentum space, at the price of increasing the number of residues and poles compared with the Adler-Adler formalism, provides an exact algorithm for the representation of neutron cross sections. Hwang¹⁴ pursued this approach and provided an elegant way of computing the parameters.

In particular, Eqs. (2-61) and (2-62) can be generalized to accommodate all higher angular momentum states beyond $l = 0$ by extending the sums to $2N(l+1)$ terms, whereby the energy dependence of the penetration factors as well as the shift factors can be accounted for.

The computer code WHOPPER¹⁴ by Hwang was used to convert the Reich-Moore resonance parameters into equivalent Adler-Adler parameters by using its POLLA¹³ option and to the multipole representation by using the POLLY option.

2.4 THEORETICAL STATISTICAL DISTRIBUTION OF THE RESONANCE PARAMETERS

Systematic measurements of the resonance widths, mainly in the case of neutron and fission widths, show strong fluctuations among resonances of the same total angular momentum and parity. It should be expected, from Eq. (2-35), that these fluctuations are connected either to the reduced widths $\gamma_{\lambda c}$ or to the penetration factors P_c . However, it is improbable that such fluctuations are due to the penetration factors because they are either constant or a smooth function of the energy. Hence, the observed fluctuations must be related to the reduced widths. This is the case shown by Porter and Thomas.¹⁰ These authors noted that the reduced widths $\gamma_{\lambda c}$, Eq. (2-13), are functions of the channel functions $\phi_c(E_\lambda, a_c)$ which, in turn, are the projection of the eigenfunctions of the compound nucleus on the nuclear surface. This projection involves the integration over the high-dimensional phase space of the compound nucleus and is made of many uncorrelated contributions which, as consequence of the central limit theorem, leads to normally distributed zero-mean sets of channel functions. Hence, from the above and Eq. (2-13), the statistical distribution function $P(\gamma_{\lambda c})$, for the reduced widths, can be written as

$$P(\gamma_{\lambda c})d\gamma_{\lambda c} = \frac{1}{\sqrt{2\pi \langle \gamma_{\lambda c}^2 \rangle}} \exp\left(-\frac{\gamma_{\lambda c}^2}{2 \langle \gamma_{\lambda c}^2 \rangle}\right) d\gamma_{\lambda c} . \quad (2-63)$$

Since quantities which appear directly in the cross-section formulae are the level widths $\Gamma_{\lambda c}$ given by sums of the square of ν normally distributed zero mean reduced width $\gamma_{\lambda c}$ with the same mean, their distribution (in view of a well-known theorem in statistical theory) must follow the χ^2 -distribution:

$$P_\nu(x) dx = \frac{\nu}{2G(\nu/2)} (\nu x/2)^{\nu/2-1} \exp(-\nu x/2) dx , \quad (2-64)$$

where $x = \Gamma_\lambda / \langle \Gamma \rangle$, $G(\nu/2)$ is the mathematical gamma function, and $\langle \Gamma \rangle$ is taken as an average over a given energy range. In the particular case of $\nu = 1$, Eq. (2-64) is the Porter-Thomas distribution.

The spacing between two consecutive resonance energies for the same total angular momentum and parity, i.e., $D_\lambda = E_\lambda - E_{\lambda-1}$, exhibits random behavior. A good representation of the level spacing distribution is provided by the Wigner law¹⁵

$$P(x)dx = \frac{\pi x}{2} \exp\left(-\frac{\pi x^2}{4}\right)dx , \quad (2-65)$$

where $x = D_\lambda / \langle D \rangle$ and $\langle D \rangle$ are the average level spacings.

Although some accurate level spacing distributions have been provided by Mehta,¹⁶ the Wigner's law is the most widely used and suitable for practical applications.

In addition to the theoretical distribution of the resonance parameter mentioned above, another very useful tool for evaluating nuclear data is the Δ_3 -statistics test derived by Dyson and Mehta.¹⁷ Δ_3 is a measure of the mean-square deviation between the number of observed energy levels and the fit of the number of levels to a straight line as a function of energy. If $N(E)$ is the number of levels observed as a function of energy in the energy interval (E_i, E_f) and the best fit straight line is $aE + b$,

$$\Delta_3 = \text{Min}_{a,b} \left[\frac{1}{E_f - E_i} \int_{E_i}^{E_f} \left(N(E) - aE - b \right)^2 dE \right] . \quad (2-66)$$

For n energy levels, the Dyson and Mehta statistics theory predicts that

$$\langle \Delta_3 \rangle = \frac{1}{\pi^2} \left[\ln(n) - 0.0687 \right] , \quad (2-67)$$

with a variance given as

$$V_{\Delta_3} = 1.169/\pi^4 . \quad (2-68)$$

CHAPTER III

EXPERIMENTAL EFFECTS

The cross-section formalism presented in Chapter II was developed assuming that the nucleus was at rest in the laboratory system and that the neutron-nucleus system was isolated. However, such assumptions do not correspond to the real case because the measured cross sections are affected by both the motion of the atoms in the target nuclei and experimental effects. From the evaluator's point of view, information on these effects is of fundamental importance in the evaluation of nuclear data. From the technical point of view, the Doppler effect is responsible for the prompt negative temperature coefficient in thermal reactors. Therefore, reactor physicists are required to consider this effect in detail to provide adequate reactor stability and inherent safety.

In this chapter we will give a brief review of the Doppler broadening of the cross section and present a new approach to calculate the Doppler broadening. Also, experimental effects such as resolution broadening, normalization, and background will be discussed.

3.0 DOPPLER BROADENING

The Doppler broadening of a cross section is a well-known effect which is caused by the thermal motion of the atoms of the target nuclei. Since the target nuclei are not at rest in the laboratory system the neutron-nucleus cross section will depend on the relative speed of the neutron and the nucleus. The relation between the cross section measured in the laboratory and the cross section which depends on the relative speed between the neutron and the nucleus is

$$v\bar{\sigma}(v) = \int |\mathbf{v} - \mathbf{V}| \sigma(|\mathbf{v} - \mathbf{V}|) P(\mathbf{V}) d\mathbf{V} , \quad (3-1)$$

where \mathbf{v} and \mathbf{V} are the incident neutron and nucleus velocities, respectively. The dependence of the cross section on the relative speed between the neutron and the nuclei is expressed in $\sigma(|\mathbf{v} - \mathbf{V}|)$ where the relative speed is $|\mathbf{v} - \mathbf{V}|$ and $P(\mathbf{V})$ is the target nuclei velocity distribution. A major problem is the choice of the appropriate velocity distribution function of the target nuclei. A Maxwell-Boltzmann velocity distribution is usually assumed for the target nuclei. Lamb¹⁸ has shown that the target nuclei have a Maxwellian velocity distribution where the temperature parameter T in the Maxwellian is not, in general, equal to the thermodynamic temperature. The Maxwell-Boltzmann distribution is given by

$$P(\mathbf{V})d\mathbf{V} = \frac{1}{\pi^{3/2}} \exp\left(-\frac{V^2}{v_T^2}\right) \frac{d^3V}{v_T^3}, \quad (3-2)$$

where $v_T^2 = \frac{2kT}{M}$, M is the mass of the target atom, k is the Boltzmann's constant ($k = 8.617 \times 10^{-5}$ eV/K), and T is the absolute temperature of the gas.

The Doppler-broadened cross section is obtained by substituting Eq. (3-2) into Eq. (3-1) and carrying out the integration on the relative velocities $\mathbf{v}_r = \mathbf{v} - \mathbf{V}$ which gives

$$\bar{\sigma}(v) = \frac{1}{\sqrt{\pi}} \int_0^\infty \frac{dv_r}{v_T} \frac{v_r^2}{v^2} \left[\exp(-(v-v_r)^2/v_T^2) - \exp(-(v+v_r)^2/v_T^2) \right] \sigma(v_r). \quad (3-3)$$

The kinetic energy of the incident neutron in the laboratory and center-of-mass system are given, respectively, as

$$E = \frac{1}{2}mv^2, \quad (3-4)$$

and

$$E_r = \frac{1}{2}\mu v_r^2, \quad (3-5)$$

and Equation (3-3) can be written as

$$\sqrt{E} \bar{\sigma}(E) = \frac{1}{\Delta \sqrt{\pi}} \int_0^{\infty} dE_r \left[\exp(-\beta(\sqrt{E} - \sqrt{E_r})^2) - \exp(-\beta(\sqrt{E} + \sqrt{E_r})^2) \right] \sqrt{E_r} \sigma(E_r) , \quad (3-6)$$

where $\Delta = \sqrt{\frac{4mkTE}{M}}$ is the Doppler width and $\beta = \frac{M}{mkT}$.

Equation (3-6) is exact within the framework of the free-gas model. As mentioned before, the temperature parameter of the free-gas model can be appropriately adjusted by the Lamb correction which will provide an effective temperature given as

$$T_{eff} = \frac{3}{2} T \left(\frac{T}{\theta} \right)^3 \int_0^{\theta/T} dx x^3 \coth \frac{x}{2} , \quad (3-7)$$

or

$$T_{eff} = T \left(1 + \frac{1}{20} \frac{\theta^2}{T^2} + \dots \right) , \quad (3-8)$$

where θ is the Debye temperature of the sample.

3.1 A FINITE DIFFERENCE METHOD FOR TREATING THE DOPPLER BROADENING OF CROSS SECTIONS

A number of numerical techniques¹⁹ have been described to approximate the integral in Eq. (3-6), but here a new approach will be introduced which is based on the finite difference method that is particularly well suited for resonance analysis and reactor applications.

A close look at Eq. (3-6) reveals that the Doppler-broadened cross section is obtained by convoluting the unbroadened cross section with the Solbrig²⁰ kernel. With the following change of variables $u = \sqrt{E}$ and $\xi = \frac{mkT}{4M}$, Eq. (3-6) becomes

$$E \bar{\sigma}(E) = \frac{1}{2\sqrt{\pi\xi}} \int_0^{\infty} du' u' \left[\exp\left(-\frac{(u-u')^2}{4\xi}\right) - \exp\left(-\frac{(u+u')^2}{4\xi}\right) \right] \sigma(u') . \quad (3-9)$$

Defining $F(u, \xi) = E\bar{\sigma}(E)$ and $\zeta = 2\xi$, Eq. (3-9) can be represented in terms of the following second-order differential equation:

$$\frac{\partial^2 F}{\partial u^2} = \frac{\partial F}{\partial \zeta} . \quad (3-10)$$

Because of the initial condition $F(u, 0)$ for $-\infty < u < \infty$ and the boundary condition $F(\infty, \zeta) = F(\infty, 0)$ and $F(-\infty, \zeta) = F(-\infty, 0)$, the function F can be calculated by use of the finite difference method.

This method consists of solving Eq. (3-10) by applying an explicit finite difference formalism assuming constant meshes with $\delta u = h$ and $\delta \zeta = \gamma$. The first and second derivatives can be expanded in a Taylor's series. The explicit finite difference equation for the function F at any u_i and ζ_{j+1} is

$$F_i^{j+1} = s(F_{i+1}^j + aF_i^j + F_{i-1}^j) , \quad (3-11)$$

where $s = \gamma/h^2$ and $a = (1 - 2s)/s$.

The stability condition²¹ of Eq. (3-11) requires that s be smaller than or equal to $1/2$. From both stability and accuracy considerations, one optimal choice of s is $s = 1/6$, whereby the error becomes the order of $\frac{h^4}{360} \frac{\partial^6 F}{\partial u^6} - \frac{\gamma^2}{6} \frac{\partial^3 F}{\partial \zeta^3}$ as can be shown by Taylor's expansion.

Successive substitution, starting with $j = 0$ in Eq. (3-11), yields

$$F_i^N = \sum_{l=0}^{2N} C_{Nl} F_{i+N-l}^0 , \quad (3-12)$$

where for successive N the coefficient C_{Nl} exhibits a Pascal triangle-like structure with symmetry with respect to $l = N$. The Pascal triangle-like behavior of C_{Nl} for succeeding values of N suggests that they can be identified with the coefficients of the trinomial expansion with generating a function of the form $(1 + aX + X^2)^N$

multiplied by s^N . By matching the coefficients of the resulting polynomial to Eq. (3-12), one obtains the expression

$$C_{NI} = s^N \sum_{i=(l+1)/2}^{\min(N,l)} (N; N-i, l-i, 2i-l) a^{2i-l} , \quad (3-13)$$

where the closed form for the pertinent trinomial coefficient is

$$(N; N-i, l-i, 2i-l) = \frac{N!}{(N-i)!(l-i)!(2i-l)} . \quad (3-14)$$

Since C_{NI} depends only on the fixed value of s , the computational efficiency can be enhanced significantly if C_{NI} is predetermined and stored before its application.

Equation (3-14) provides useful physical insight to the analytical behavior of C_{NI} . The quantity C_{NI} is a monotonically increasing function of l for all $l \leq N$ and becomes vanishingly small for all large $|l - M|$ when M is large. The latter is of great practical importance since it implies that only a few terms need be considered even if M is large under the condition of extreme Doppler broadening.

A simple analytical expression for asymptotic C_{NI} can be deduced readily by using the convolution integral representation of F . The discretized version of the latter over the constant mesh spacings previously defined is

$$\begin{aligned} F(u_i, \zeta) &= \frac{1}{2(\pi\zeta)^{1/2}} \int_{-\infty}^{\infty} dy \exp[-(u_i - y)^2/4\zeta] F(y, 0) \\ &= \sum_{l=i-L}^{i+L} \left[\left(\frac{3}{2\pi N} \right)^{1/2} \exp\left(-\frac{3(l-i)^2}{2N}\right) \right] F(y_l, 0) , \end{aligned} \quad (3-15)$$

where C_{NI} asymptotically approaches the quantity inside the braces for all l close to i as N becomes large. Numerical calculations have shown that Eqs. (3-15) and (3-12) become equivalent for practical purposes for all $N \geq 50$. Rigorous proof, in principle, can also be derived by using the asymptotic expressions of factorials and by Taylor's expansion around N . Thus, it becomes obvious that, as a natural

consequence implied by the Gauss kernel, only initial points not too far from the point in question will contribute to the broadening process for practical purposes. For practical applications, L in Eq. (3-15) seldom exceeds 250 even under extreme broadening conditions. The analytical behavior of C_{NI} effectively prevents the potentially excessive number of terms required by the explicit representation with fixed s .

The method has been tested against an often used approximation of the Solbrig's kernel which has a Gaussian form. For energy above 1 eV, the two methods give the same result, but the results differ considerably for very low energies. Table 3-1 shows the value of the ^{235}U total, fission, and capture cross sections broadened to 300 K at the thermal energy (2200 m/s) when calculated by the finite difference technique (method A) and by the Solbrig's kernel (method B). As can be seen, the difference can be as high as two barns as in the case of the total cross section. Figure 3-1 shows a graphical comparison of the ^{235}U fission cross section above 1 eV, in which the two methods give indistinguishable results.

Table 3-1. Numerical comparison of the two methods

	Method A	Method B	Method A - Method B
Total	698.10	700.30	2.2
Fission	584.95	586.88	1.93
Capture	98.78	99.12	0.34

The method has been implemented in the computer code SAMMY as an alternative to calculate the Doppler broadening of cross sections. It is slower but more accurate when calculating the Doppler effect for very low energies.

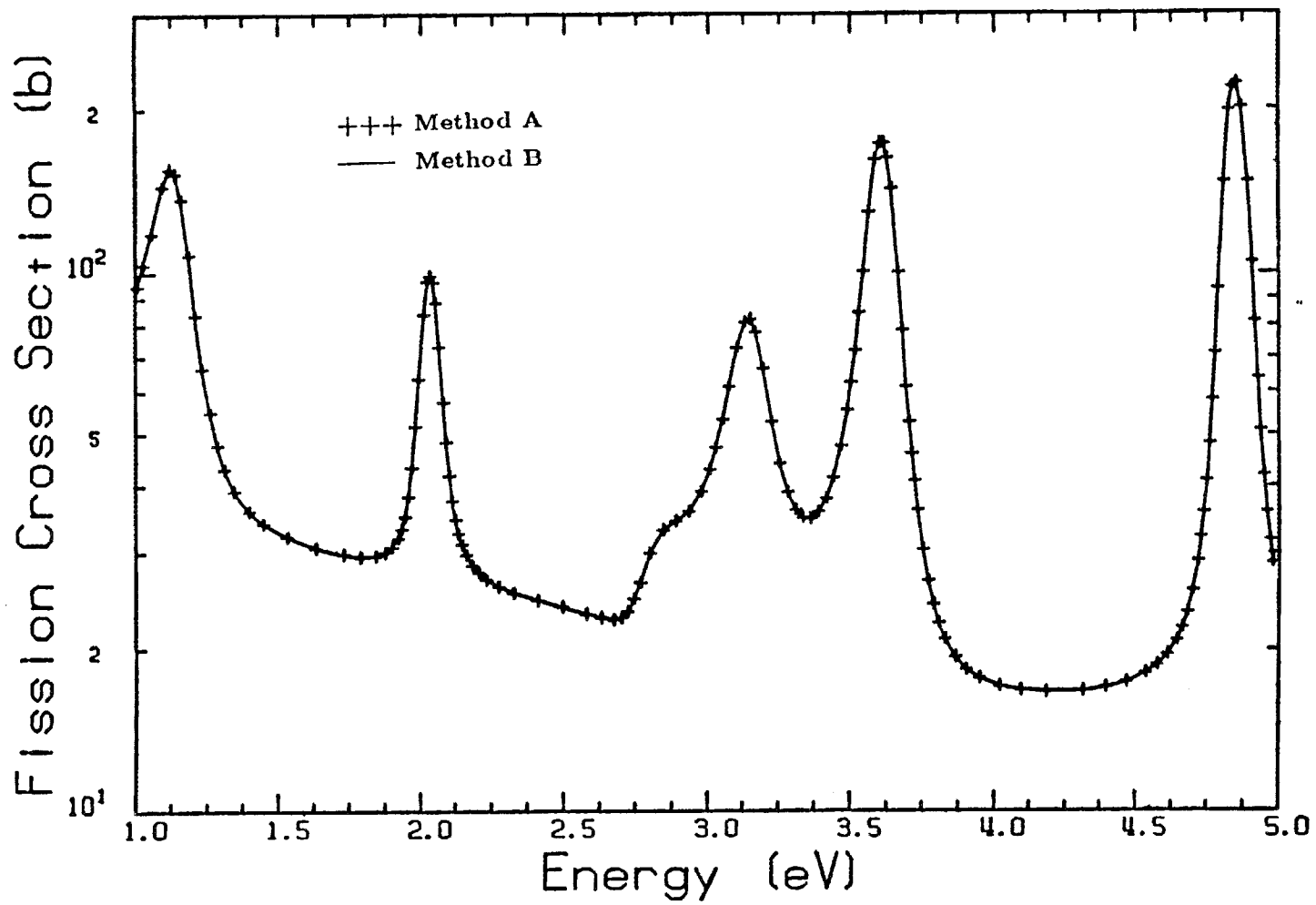


Fig. 3-1. ^{235}U fission cross section broadened to 300 K and calculated by the two methods.

3.2 RESOLUTION BROADENING

Measured cross sections are not only Doppler broadened but are also resolution broadened by the finite energy resolution of the measuring detector.²² The main causes for instrumental broadening are the spread in the flight paths due to the effective thicknesses of the detector and the moderator, the uncertainty in the flight time associated with the spread in the moderation times and with the width of the neutron burst, and the time channel at the detector. We will consider the broadening effect due to the neutron burst and the time channel at the detector. The broadening due to other effects, such as jitters and the time resolution of the detector, is much smaller and can often be neglected.

Similar to the Doppler-broadening effect, the effect of the instrumental resolution is obtained by convoluting the cross section with a Gaussian kernel. The resolution effect on the measured cross section is given as

$$\sqrt{E} \bar{\sigma}(E) = \frac{1}{\Delta^* \sqrt{\pi}} \int_0^\infty dE_r \exp\left(-\left(\frac{E - E_r}{\Delta^*}\right)^2\right) \sqrt{E_r} \sigma(E_r) , \quad (3 - 16)$$

where the resolution width due to the instrumental effect is given as

$$\Delta^* = \sqrt{\frac{2(s^2 + \delta L^2)}{3L^2} E^2 + \frac{2(\delta t_b^2 + t^2)}{3\mu^2 L^2} E^3} , \quad (3 - 17)$$

L is the flight path, δL is associated to the uncertainty in the position in which the neutrons are born in the moderator, s is the sample effective thickness, δt_b is the neutron burst width, t is the variable channel width, and μ is a constant whose value is $72.3 \text{ eV}^{1/2} \mu\text{sec}/\text{m}$.

3.3 NORMALIZATION AND RESIDUAL BACKGROUND

In the resonance region, experimenters²² usually measure the shape (energy dependence) of the cross section relative to another cross section (the standard)

whose shape is known. For instance, ^{10}B and ^6Li have an $1/v$ cross-section shape in the resonance region. The cross-section shape must then be normalized at some point where its absolute value is known. The absolute value of cross sections are usually best known at the thermal energy (0.0253 eV). There is always a small systematic uncertainty associated with the normalization of a measured cross section. When analyzing simultaneously several related cross sections (fission, capture, total), it is often desirable to search for a normalization constant that optimizes the consistency of the related cross sections.

There are always backgrounds associated with cross-section measurements. An important source of background is due to the detection of spurious events caused by stray neutrons in the experimental environment. Experimenters have techniques to estimate those backgrounds to correct the measurements; however, there always remains an uncertainty associated with the background correction. Therefore, in some cases it is desirable to search for a possible small residual background when analyzing cross sections.

CHAPTER IV

METHOD OF EVALUATION

Nuclear data evaluation is an elaborate process which requires several stages of development. These stages consist of (1) the gathering of detailed information on the experimental conditions associated with the measurements, (2) the choice of the set of measurements to be included in the evaluation, and (3) the selection of the interaction model which adequately describes the neutron-nucleus reaction.

In the evaluation of the ^{235}U neutron cross sections, several data were examined for inclusion in the analysis. They were transmission data (total cross section), fission cross-section data, and capture cross-section data. The spin-separated fission cross-section data obtained from the analysis of polarized neutron/polarized target were incorporated in the evaluation to assign each s-wave resonance to the proper spin state. The spin-separated data combined with the Δ_3 -statistics method provided a very powerful technique for the assignment of the spin of the resonance as well as resolving the resonance structure.

The computer code SAMMY⁵ which accommodates the reduced R -matrix Reich-Moore formalism was utilized in the evaluation. The fitting procedure of the SAMMY code is based on the Bayes' method and allows the successive incorporation of new data in a consistent manner.

In this chapter we will present the method of analysis utilized in the evaluation of the ^{235}U neutron cross sections by describing the experimental data, the data reduction, and the resonance analysis.

4.0 SELECTION OF DATA

Various sets of measurements were examined for inclusion in the evaluation of the ^{235}U neutron cross sections. Most of the neutron cross-section measurements in the CSISRS file² or in the CINDA index³ were investigated, and the choice of measurements was based on the information available on the data. High-energy resolution and detailed information on the experimental conditions and the uncertainties were the main criteria in the data selection. Eleven measurements were selected as shown in Table 4-1. Seven fission data were chosen to cover the energy range relevant to the present analysis. The spin-separated data of Moore et al.²³ were chosen to provide a consistent way of assigning the *s*-wave resonance spin. The low-energy fission data of Wagemans et al.²⁴ were found to be useful in determining the values of the fission cross section at a thermal energy of 0.0253 eV. The 50-m flight path, liquid-nitrogen-cooled sample measurement of Blons²⁵ was included because of its good instrumental resolution and reduced Doppler broadening. Unfortunately, the Blons data have a large residual background, and the energy dependence of the cross section was not quite consistent with most of the other data sets. Two sets of fission cross-section data of Weston and Todd^{26,27} which were taken in two different flight paths (namely, 18.9 m and 86.5 m) were used in the analysis. The 86.5-m measurement was particularly useful for resolving the resonance structure above 50 eV. The fission cross-section data of Gwin et al.²⁸ and Schrack²⁹ were used mostly below 20 eV because of the poor energy resolution at higher energies.

Four transmission measurements were taken into account in the analysis. The transmission data of Spencer et al.³⁰ at low energy were used to determine the shape of the total cross section below 1 eV and to determine the value of the

Table 4-1. Selected measurements of the ^{235}U neutron cross sections

Reference	Energy range used in the analysis	Measurement characteristics
Wagemans et al. ²⁴ (1988)	0.001 to 0.4 eV	Fission at 8 m
Gwin et al. ²⁸ (1984)	0.01 to 20 eV	Fission at 25.6 m
Blons ²⁵ (1973)	17 to 500 eV	Fission at 50 m; sample cooled to 77 K
Weston and Todd ²⁶ (1984)	14.0 to 100 eV	Fission at 18.9 m
Weston and Todd ²⁷ (1988)	100 to 500 eV	Fission at 86.5 m
Schrack ²⁹ (1988)	0.02 to 20 eV	Fission at 8.4 m
de Saussure et al. ³² (1967)	0.01 to 50 eV	Capture at 25.5 m
Spencer et al. ³⁰ (1984)	0.01 to 1 eV	Transmission at 18 m. Sample of 0.001468 atom/b.
Harvey et al. ³¹ (1986)	0.4 to 68 eV	Transmission at 18 m. Sample cooled to 97 K. Sample of 0.03269 atom/b.
Harvey et al. ³¹ (1986)	4 to 500 eV	Transmission at 80 m. Samples cooled at 97 K. Samples of 0.002335 and 0.03269 atom/b.
Moore et al. ²³ (1978)	1.6 to 100 eV	Separated spin states fission data.

cross section at thermal energy. Three transmission data of Harvey et al.³¹ with different sample thicknesses were analyzed. The data include measurements done on the 18- and 80-m flight paths with sample thicknesses of 0.002335 and 0.03269 atom/b and with the sample cooled at the liquid-nitrogen temperature to reduce the Doppler broadening of the resonances. The low-resolution measurements done

on the 18-m flight path were used from 0.4 eV to 68 eV. The high resolution measurements done on a flight path of 80 m were used in the range of 4 eV to 500 eV. These measurements provided the best resolution data available and were taken as a standard in the analysis.

Simultaneous measurements of fission and capture data of de Saussure et al.³² provided capture cross-section data used in the analysis.

4.1 DATA REDUCTION

Most contemporary neutron cross-section measurements in the resonance energy region are done by the time-of-flight (TOF) technique. Pulses of neutrons are collimated on a flight path, and the time intervals between the neutron pulses and the events at the detector at the end of the flight path are recorded. The neutron energy E can be obtained from the time of flight t_n and the effective flight path L by the relation

$$E_n = \mu^2 \frac{L^2}{t_n^2} , \quad (4-1)$$

where $\mu = 72.3 \text{ eV}^{1/2} \mu\text{sec}/\text{m}$.

Intense bursts of fast neutrons are often produced with pulsed electron linear accelerators. Pulses of 100-MeV electrons are stopped in a water-cooled metal target where they produce fast neutrons by the (γ, n) reaction. Some of the neutrons are slowed down by the water moderator surrounding the target.

If L and t_n are not correlated, the energy resolution in a time of flight experiment can be obtained from Eq. (4-1) as

$$\frac{\Delta E_n}{E_n} = 2 \left[\left(\frac{\Delta t_n}{t_n} \right)^2 + \left(\frac{\Delta L}{L} \right)^2 \right]^{1/2} , \quad (4-2)$$

where t_n is the flight time of the neutrons of energy E_n over path length L . The source of uncertainty in t_n and in L was explained in Section 3.2.

The uncertainty in the time t may be calculated as follows:

$$\Delta t_n = \sqrt{\Delta t_{cw}^2 + \Delta t_{bw}^2} , \quad (4-3)$$

where Δt_{cw} is the channel width, and Δt_{bw} is the burst width. Since SAMMY requires a Gaussian instead of a rectangular width, Δt_n is converted to an equivalent Gaussian width as

$$\Delta t_G = 0.67978 \Delta t_n . \quad (4-4)$$

The broadening due to the moderation at ORELA was computed by the Monte Carlo method by Coceva et al.³³ In the 30 to 300 eV range it corresponds to a flight-path spread of 0.022 m. The broadening due to multiple scattering in the Li glass detector used in the ORELA transmission measurements was computed by Perey et al.³⁴ and is equivalent to an exponential tail of 22 ns in the response function.

Besides the resolution effects, another source of error in the measured cross section may be due to contaminants on the sample target. The 0.03269 atom/b transmission sample measurement of Harvey et al. contained impurities of ^{151}Ta , ^{234}U , ^{236}U , and ^{238}U for which the transmission data had to be corrected. This was done by computing the transmission due to these impurities, using published resonance parameters,³⁵ and correcting the measurements for their effect.

Another correction to the transmission measurements which had to be considered was due to the variation in the sample size or the sample density with sample temperature. This correction was computed using the data of reference 36. The ratio of the area density of the uranium at liquid nitrogen temperature to the area density at room temperature was found to be

$$\frac{\rho T}{\rho_0} = 1.0057 , \quad (4-4)$$

where ρ_T is the area density of the sample calculated at the liquid nitrogen temperature, and ρ_0 is the area density at room temperature.

4.2 RESONANCE ANALYSIS

Resonance parameter analyses of the selected experimental data of ^{235}U were performed utilizing the multilevel reduced R -matrix Reich-Moore formalism option of the Bayesian computer code SAMMY. The Bayesian approach allows the consistent successive incorporation of new data in the analysis. The option to search not only for resonance parameters but also for experimental parameters such as sample thicknesses, sample effective temperatures, backgrounds, normalizations, and parameters of the instrumental resolution, all consistent with predetermined uncertainty limits, leads to realistic uncertainties and covariance matrices.

The first step in the resonance analysis procedure is to determine the quantum selection rule. Pertaining to the neutron- ^{235}U interaction, the spin of the neutron and ^{235}U are, respectively, $i = 1/2$ and $I = 7/2$ which provides for the spin of the compound nucleus $S = 3$ and $S = 4$. The total angular momentum of the compound nucleus can have values between $J = |L - S|$ and $J = L + S$ where L is the relative neutron-nucleus angular momentum. For s -wave ($L = 0$) the total angular momentum can be $J = 3$ and $J = 4$. We have assumed that all the resonances observed below 500 eV were s -waves ($L = 0$). The p -wave ($L = 1$) penetration factor $\rho^2/(\rho^2 + 1)$ is 1.6×10^{-3} at 500 eV; hence, a few of the smaller resonances observed may be p -wave. However, the existing experimental data do not permit discriminating between small s -wave resonances and large p -wave resonances.

The first challenge of evaluators in evaluating cross-section data is the construction of an initial set of resonance parameters. Usually the resonance energy,

the channel widths, and the resonance spin are the quantities required for the construction of a resonance parameter set. The parameters entering the multilevel Reich-Moore formalism are: energy level E_r , gamma capture width Γ_γ , neutron width Γ_n , fission width which is assumed to be comprised of two channels Γ_{f1} and Γ_{f2} for each spin, and the spin of the resonance J . It is obvious that a good initial estimate of the resonance parameters will require high-resolution data. Since the level shift is zero for s -wave, the measured resonance energy is the same as the energy eigenvalue seen in Eq. (2-43). Hence, high-resolution measurements can be used to determine the energy of resonances. The high-resolution data of Harvey et al., with samples cooled at liquid nitrogen temperature and a flight path of 80 m, were chosen to determine the position of the energy levels. Also, below 50 eV information on the resonance parameters of Moore et al.²³ and Reynolds³⁷ was used as initial estimates.

The following procedure was followed to construct the set of resonance parameters. Spin-separated data of Moore et al. were graphically superimposed on the 80-m flight path thick sample transmission data of Harvey et al. so the spin state J could be assigned to each observed resonance or cluster of resonances. To confirm the existence of a resonance at a given energy and spin state the Δ_3 -statistics test of Dyson and Mehta was used. For energies above 100 eV where both spin-separated and transmission data were insufficient to resolve the observed cross-section structure, the Δ_3 -statistics method proved to be very helpful in assigning both the spin and energy of the resonance. The neutron widths were fitted to reproduce the high-resolution transmission data, and the fission widths were fitted to the fission data of Weston and Todd. The capture widths were initially fixed at 35 meV and later varied. This procedure was iterated until parameters were obtained that gave a reasonably good representation of all the data.

CHAPTER V

RESULTS OF THE ANALYSIS

The analysis of the ^{235}U neutron cross sections provided a set of resonance parameters which described the cross sections up to 500 eV. The set of Reich-Moore-type resonance parameters consists of 912 s -wave levels of which four are bound levels with energies between -100 and 0 eV. To mock up the contributions of the truncated levels above 500 eV in the energy range 0 to 500 eV, fictitious levels were added at 500.3 eV, 501.5 eV, and 550 eV. Of the 905 actual s -wave levels in the range 0 to 500 eV, 356 correspond to $J = 3$ and 549 to $J = 4$. The value of 9.94 f was obtained for the scattering radius. The set of Reich-Moore resonance parameters were also converted to equivalent Adler-Adler and multipole representations. As stated in Chapter II, the Adler-Adler representation is not exactly equivalent to the Reich-Moore representation since it neglects the energy variation of the total width of the resonance. However, the two representations are nearly equivalent as long as the neutron widths are small compared to the total widths, which is the case for ^{235}U below 500 eV. Parameters for the three representations are given in Appendix C for a few resonances. The complete set of resonance parameters are available from the author or can be requested from the National Nuclear Data Center at Brookhaven National Laboratory.¹ From the reactor computation viewpoint, it should be mentioned that the different representations of the resonance parameters provide the reactor physicist with flexibility to carry out calculations. As an example, the Adler-Adler formulation and the multipole expansion might be more convenient for the calculation of the Doppler-broadened and self-shielded cross sections using J-function¹⁹ and Voigt profiles.¹⁹

The purpose of this chapter is to present the results of the analysis by graphical and tabular comparisons between the data and the theoretical calculations using the resonance parameters. The statistical distributions of the resonance parameters are also compared with the theory.

5.0 GRAPHICAL AND TABULAR COMPARISON WITH THE DATA

Comparison of the theoretical calculations, using the resonance parameters obtained by a Bayesian analysis and the selected measurements discussed in Chapter IV and listed in Table 4-1, is shown in graphical and tabular form. The theoretical results presented in graphical form are given as solid lines whereas the data are represented by vertical lines which are one standard error high.

Figure 5-1 shows a comparison of the cross sections computed with the resonance parameters (solid line) with the total cross section of Spencer et al.,³⁰ the fission cross section of Gwin et al.,²⁸ and the fission cross section of Wagemans et al.²⁴ below 1 eV. The fission cross-section data of Gwin et al. and the total cross-section data of Spencer et al. were displaced for clarity of display as indicated in the graph. This energy range is important for the prediction of thermal reactor parameters, and, therefore, an accurate knowledge of the cross sections is desired. Table 5-1 shows the cross-section values computed at a thermal energy of 2200 m/s, Doppler broadened at 300 K using the method introduced in Chapter III and compared to the ENDF/B-V values, and compared to the values proposed by the ENDF/B-VI standards committee.³⁸

Figures 5-2 to 5-5 provide comparisons between the high resolution transmission data of Harvey et al.³¹ and the corresponding theoretical calculations. The

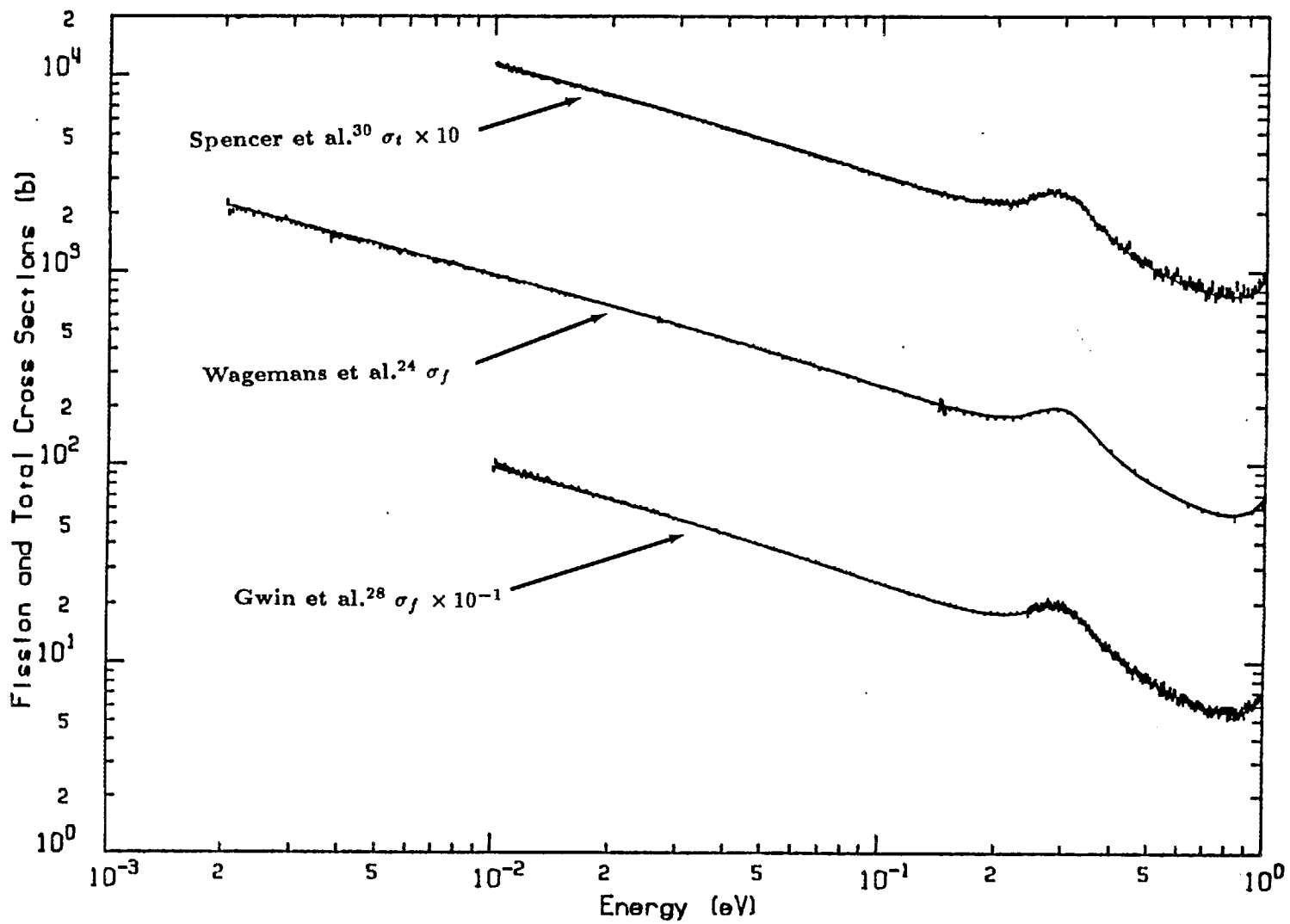


Fig. 5-1. Comparison of the total cross-section data of Spencer et al.,³⁰ the fission cross-section data of Gwin et al.,²⁸ and Wagemans et al.²⁴ with calculations using the resonance parameters.

Table 5-1. 2200 m/s value of cross sections at 300 K (b)

	This work	ENDF/B-V	Proposed standard*
Total	698.10	694.64	698.67 ± 1.71
Scattering	14.37	14.74	15.46 ± 1.06
Absorption	683.73	681.90	683.22 ± 1.34
Fission	584.95	583.52	584.25 ± 1.11
Capture	98.78	98.38	98.96 ± 0.74

*Accepted for ENDF/B-VI, except for tentative uncertainties.

transmission data correspond to three different sample thicknesses with the sample cooled to liquid nitrogen temperature to reduce the Doppler broadening. Up to 60 eV the measurements corresponding to 0.03269 atom/b at the 80-m flight path and 0.002335 atom/b at the 80-m flight path were displaced by 0.5. A search of the temperature parameter entering the Maxwellian distribution provided an effective temperature of 103.33 K.

Figure 5-6 gives a comparison between the fission cross sections of Gwin et al. and those of Schrack²⁹ with the theoretical calculations. The data of Gwin et al. were displaced by two decades for clarity of display.

Figures 5-7, 5-8, and 5-9 show comparisons of the fission cross sections of Blons,²⁵ and Weston and Todd²⁶ with calculations performed with resonance parameters. As expected, the Blons data have better resolution, but a large background can be seen in the valleys between the two consecutive resonances. In Appendix D we present values obtained for the residual background and normalization calculated with the code SAMMY. For clarity, the data of Weston and Todd were displaced by two decades as indicated.

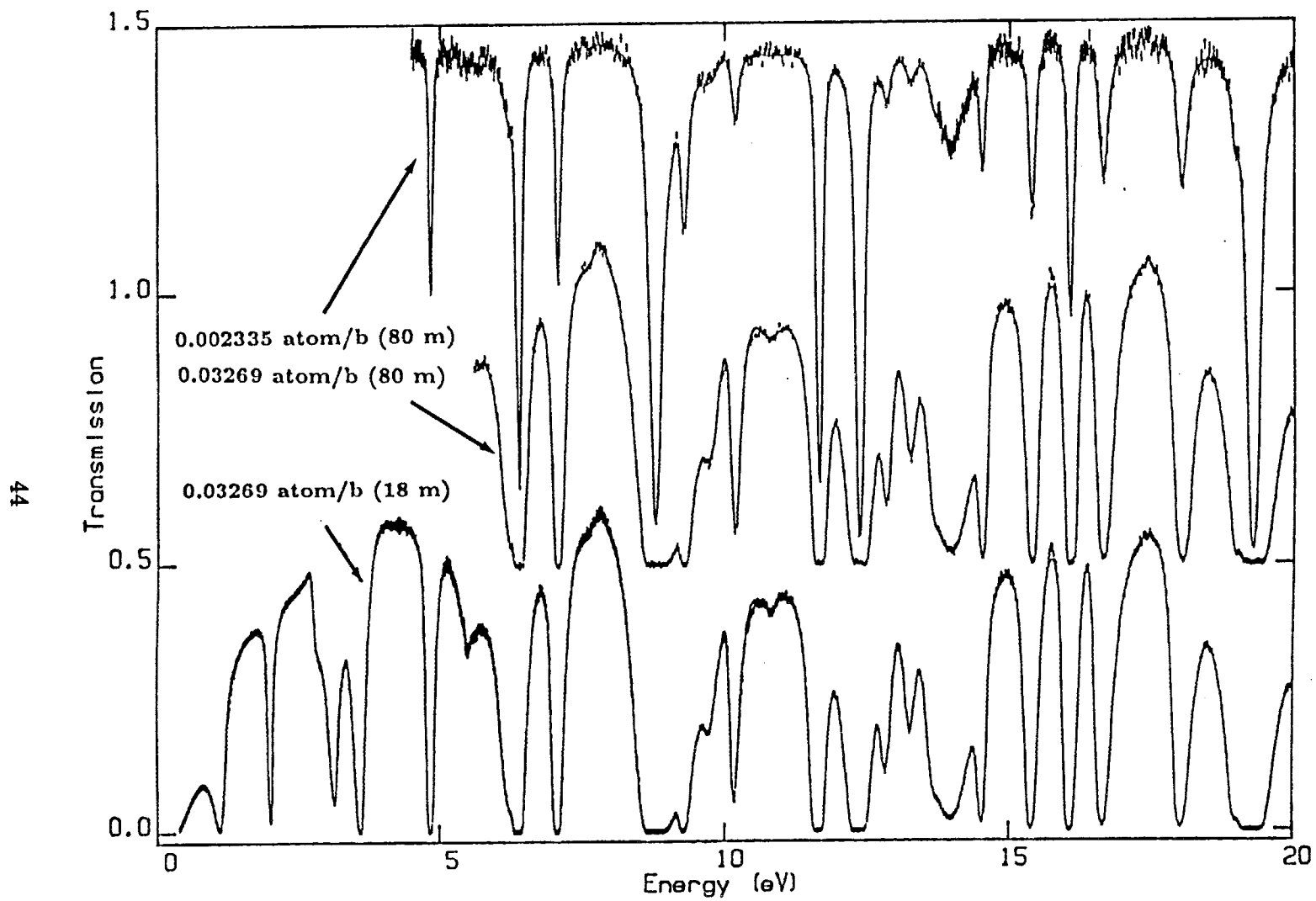


Fig. 5-2. Comparison of the transmission data of Harvey et al.³¹ with calculations using the resonance parameters. The two upper curves have been displaced upward by 0.5 for clarity.

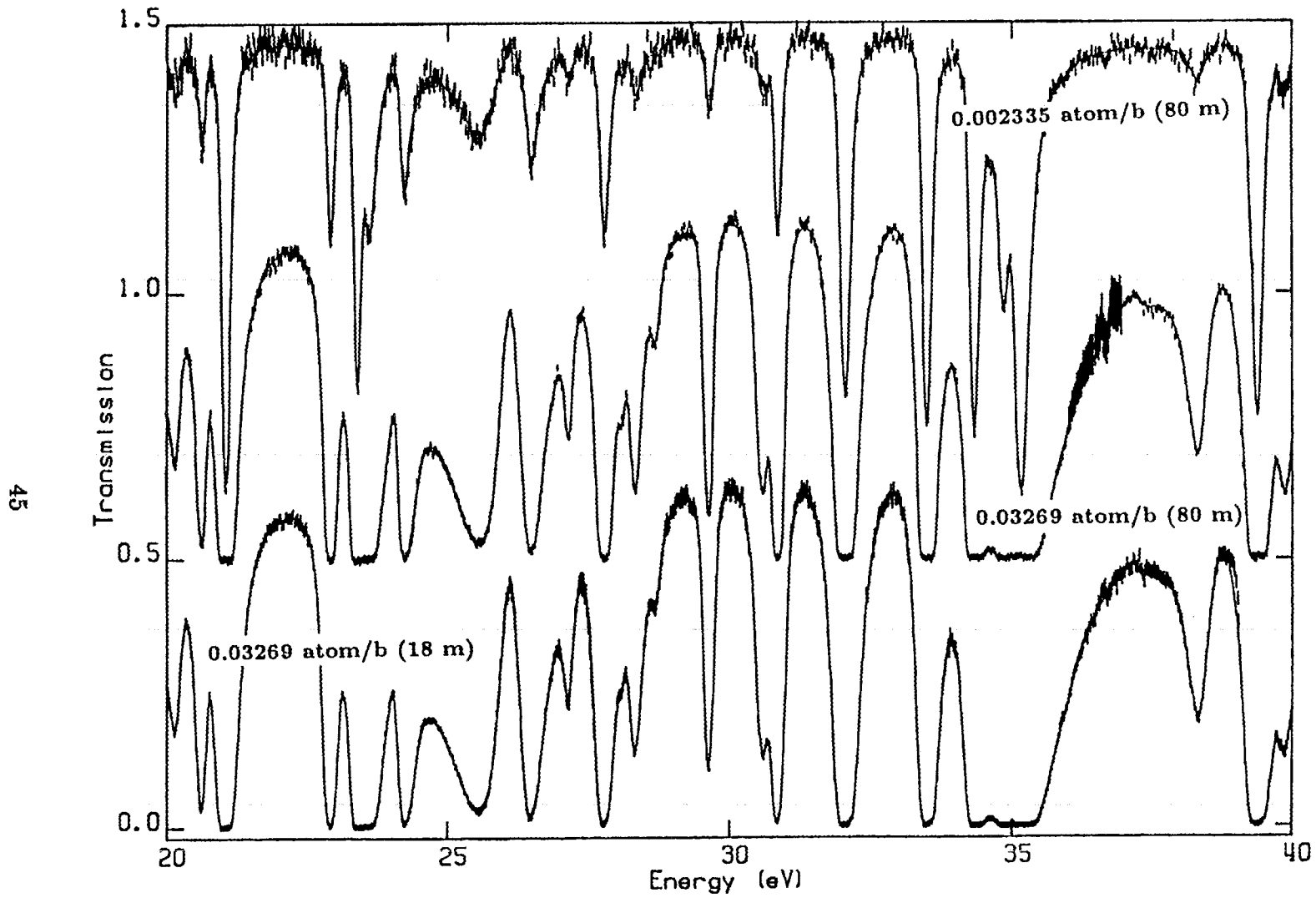


Fig. 5-3. Comparison of the transmission data of Harvey et al.³¹ with calculations using the resonance parameters. The two upper curves have been displaced upward by 0.5 for clarity.

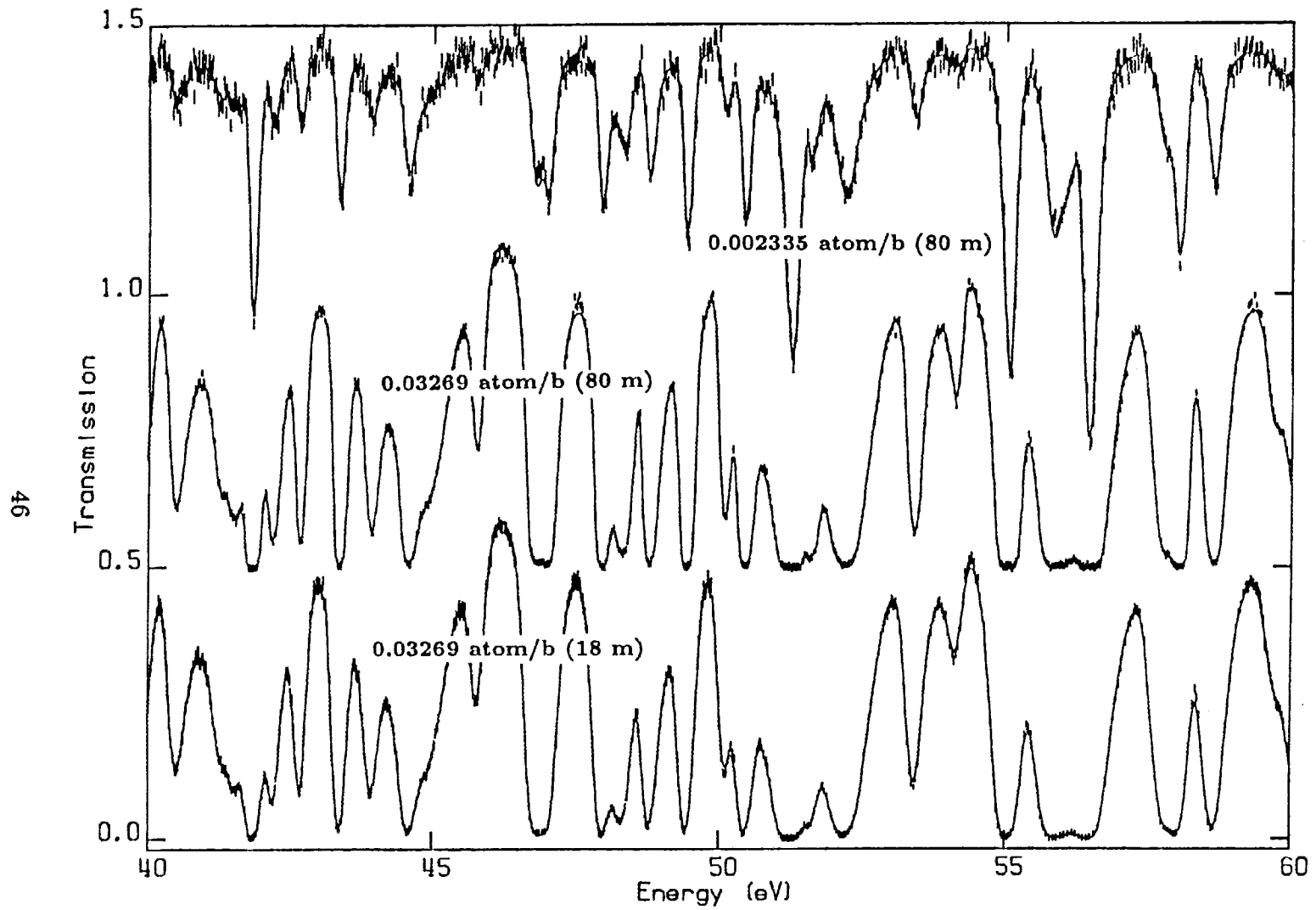


Fig. 5-4. Comparison of the transmission data of Harvey et al.³¹ with calculations using the resonance parameters. The two upper curves have been displaced upward by 0.5 for clarity.

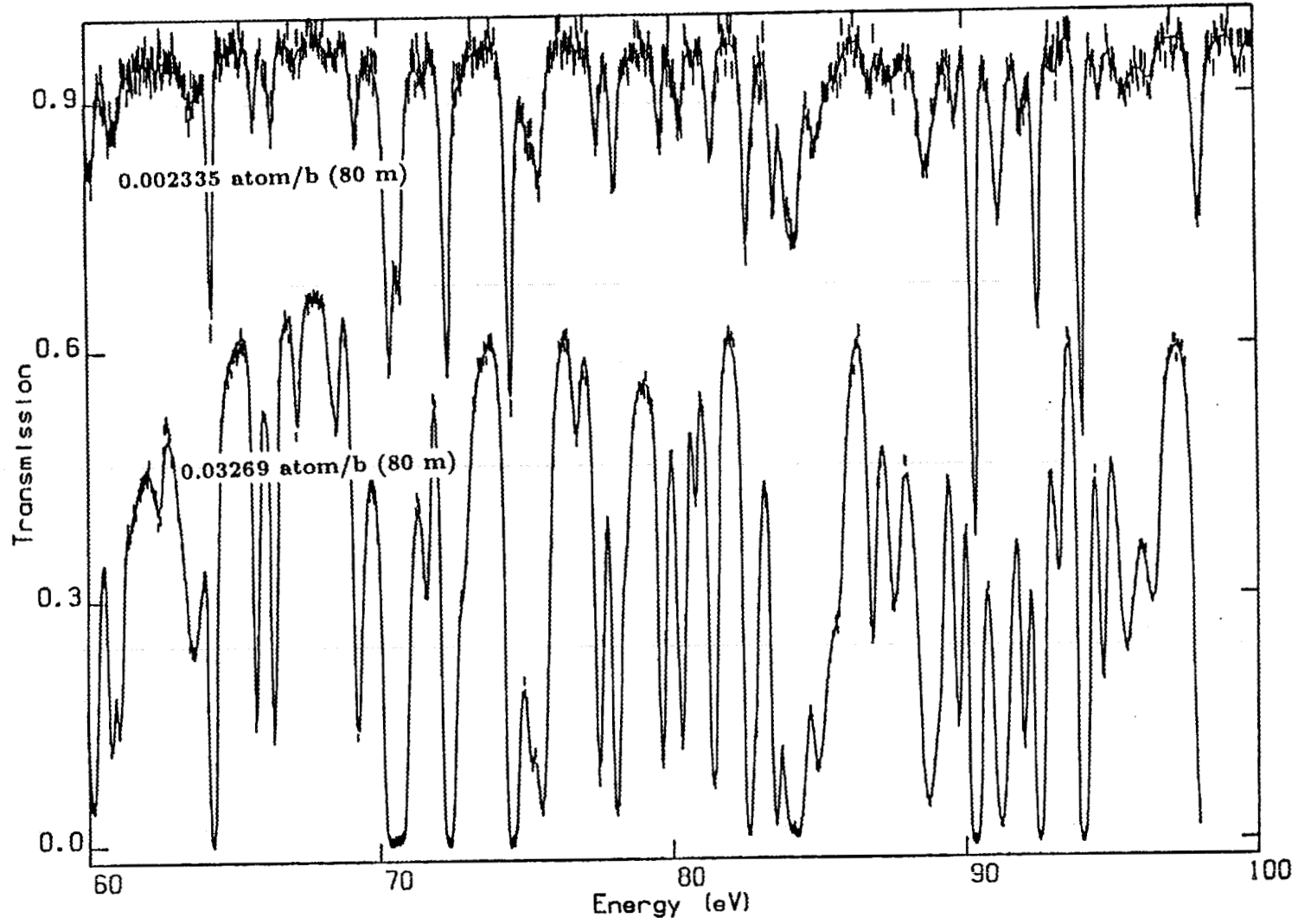


Fig. 5-5. Comparison of the transmission data of Harvey et al.³¹ with calculations using the resonance parameters.

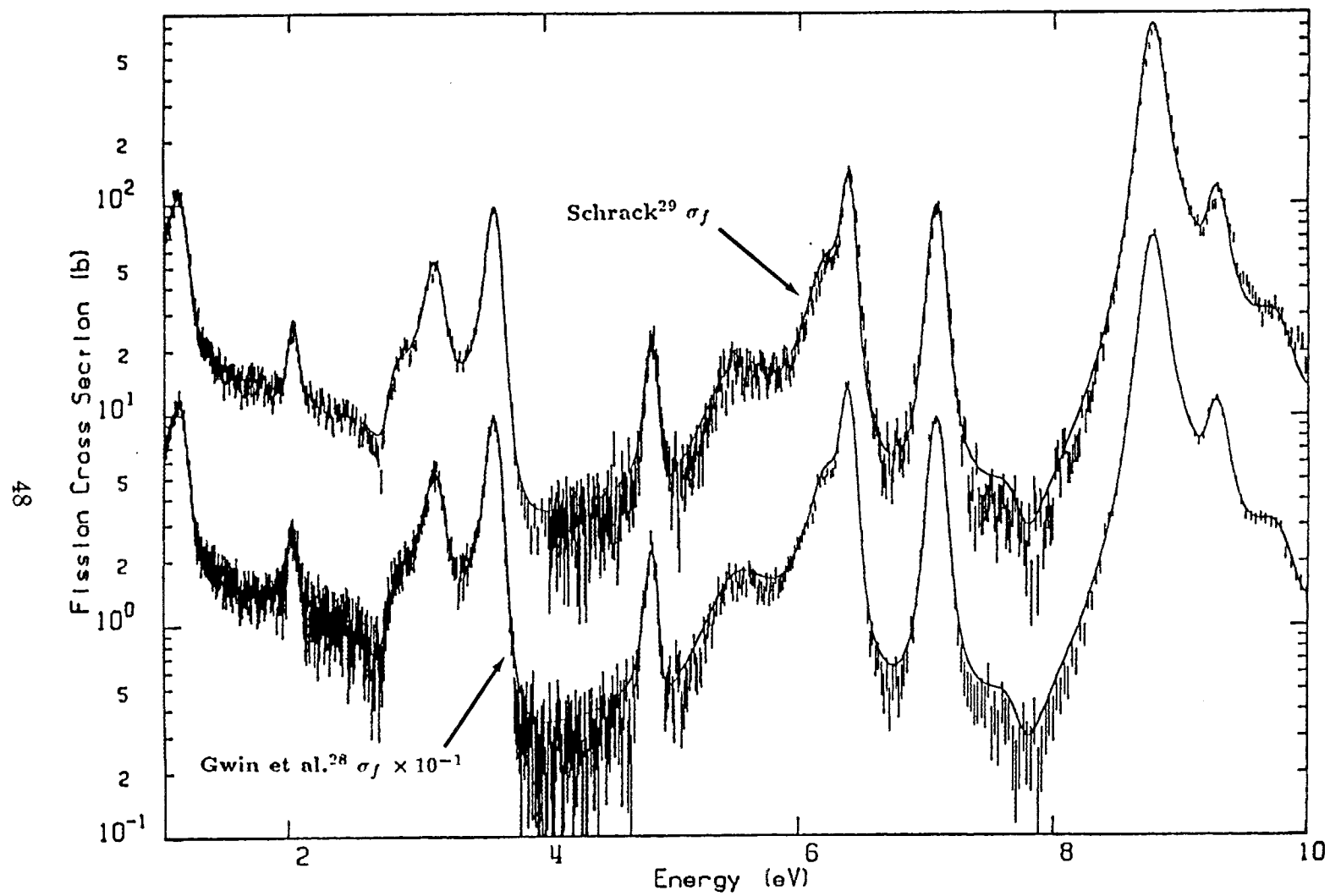


Fig. 5-6. Comparison of the fission cross-section data of Schrack²⁹ and of Gwin et al.²⁸ with calculations using the resonance parameters.

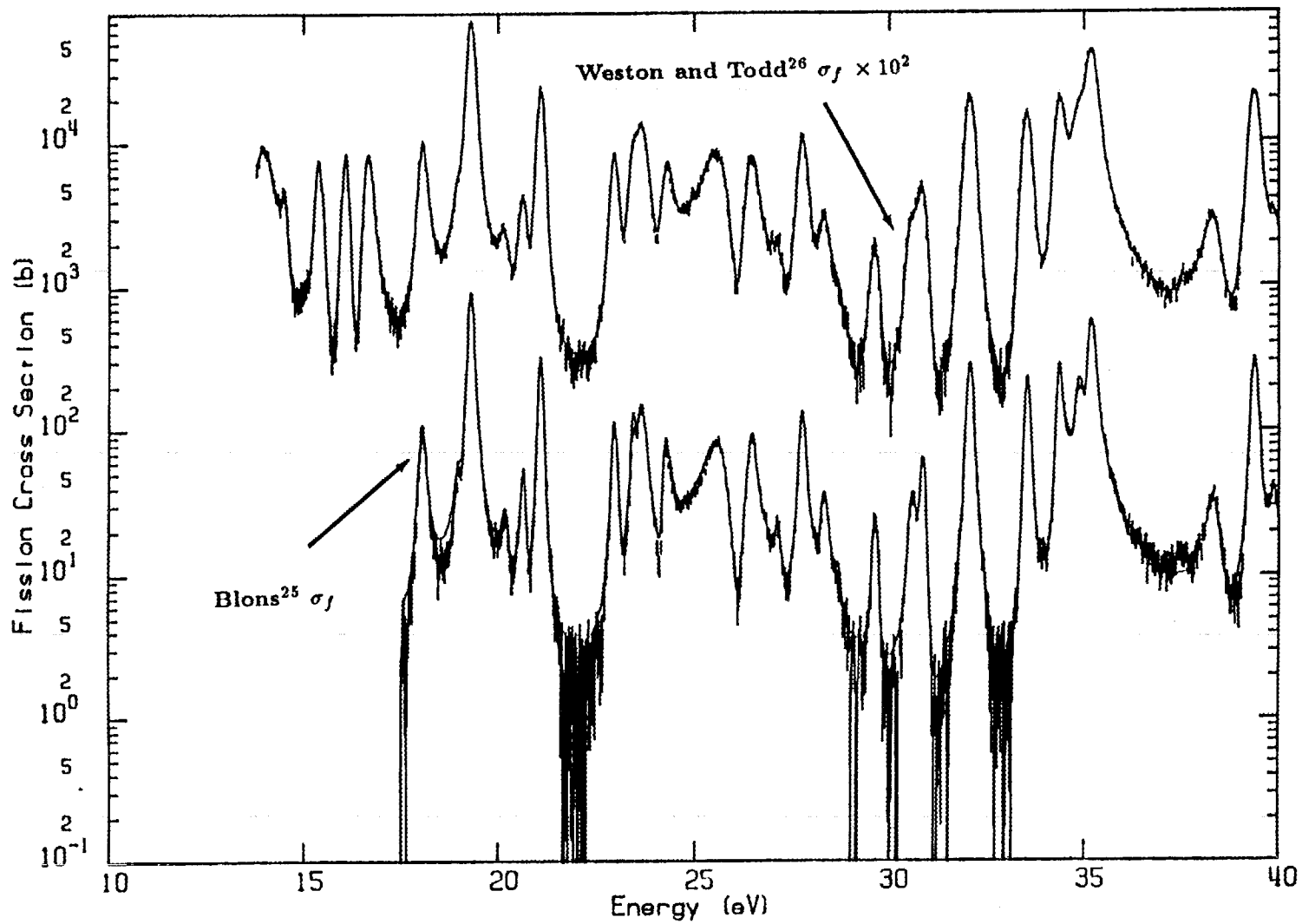


Fig. 5-7. Comparison of the fission cross-section data of Blons²⁵ and of Weston and Todd²⁶ with calculations using the resonance parameters.

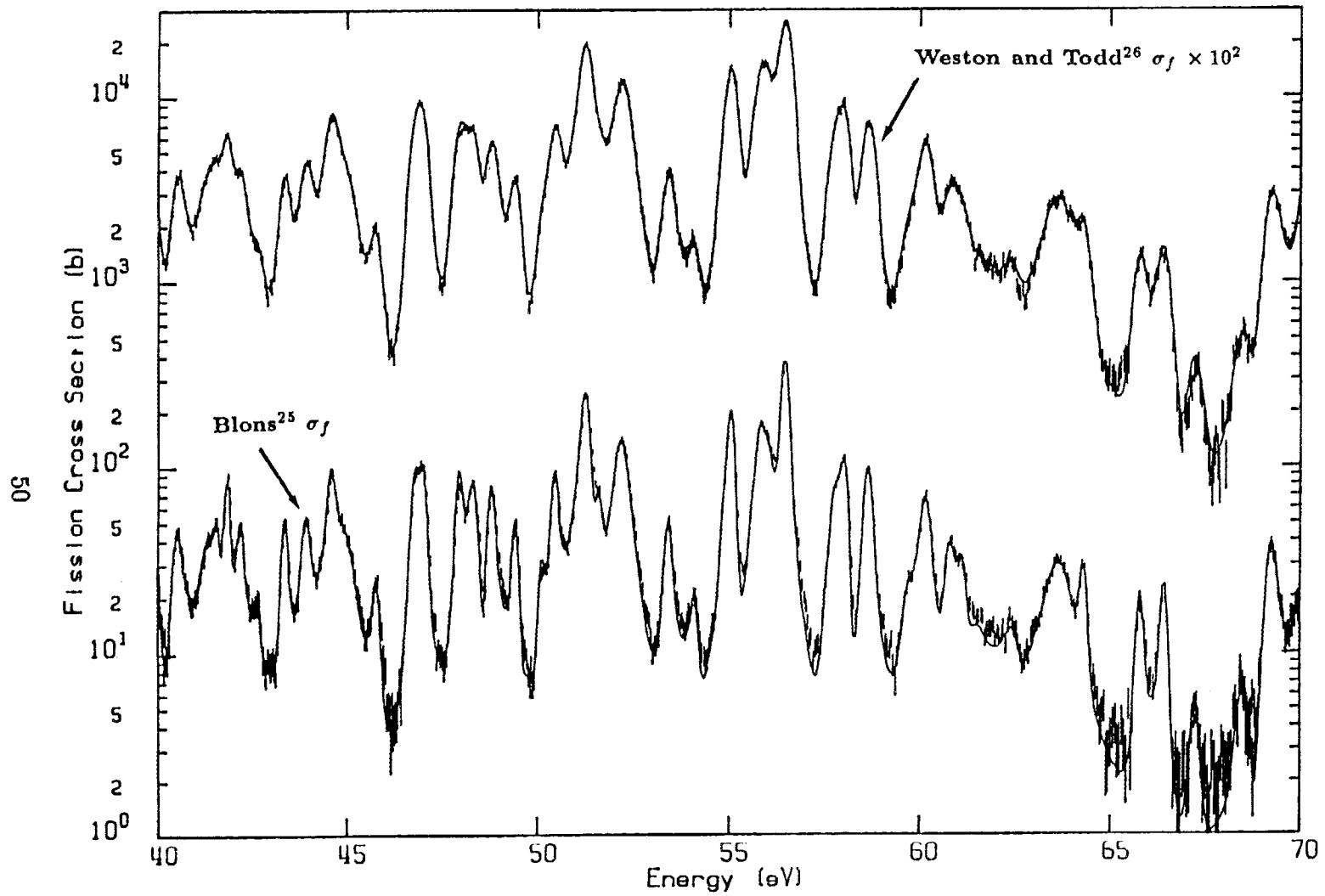


Fig. 5-8. Comparison of the fission cross-section data of Blons²⁵ and of Weston and Todd²⁶ with calculations using the resonance parameters.

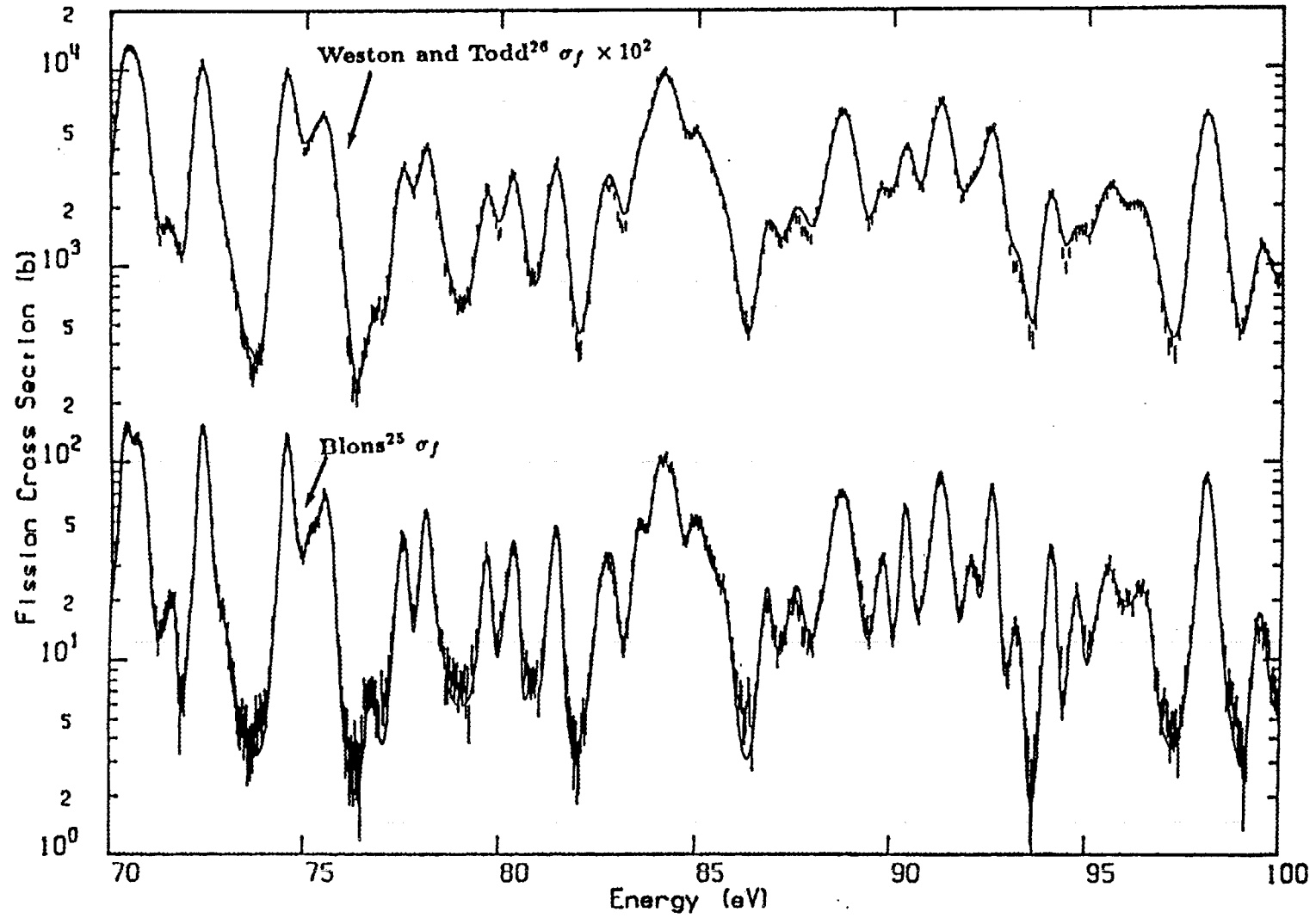


Fig. 5-9. Comparison of the fission cross-section data of Blons²⁵ and of Weston and Todd²⁶ with calculations using the resonance parameters.

Figures 5-10 and 5-11 show the spin-separated fission cross-section data of Moore et al.²³ compared with the calculations done with the resonance parameters. These data, combined with the technique developed using the Δ_3 -statistics which will be explained in Section 5.2, were used to assign each resonance to the proper spin state. As mentioned, the presence of the p -wave below 500 eV is hindered since the p -wave penetration factor is small and, hence, the cross sections are predominantly due to s -wave. Thus, fission cross sections are given by the sum of the two partial fission cross sections corresponding to the spin state $J = 3$ and $J = 4$, respectively.

Figure 5-12 shows a comparison of the capture cross-section data of de Saussure et al.³² with calculations performed with the resonance parameters.

Table 5-2 shows comparisons between the integrated fission and capture cross sections calculated with the resonance parameters and the data up to 110 eV. The fission and capture cross-section data are those of Gwin et al. and Wagemans et al., and the capture cross-section data are that of de Saussure et al.

Table 5-2. Comparison of ^{235}U integrated cross sections $\int \sigma dE$ (b eV)

Interval (eV)	Fission			Capture	
	This work	Gwin et al. ²⁸	Wagemans et al. ²⁴	This work	de Saussure et al. ³²
0.0206 – 0.06239	19.16	19.260*	$19.26 \pm 0.08^*$	3.21	
7.8 – 11.0	245	247.4	246 ± 2.5	83.71	85.16
0.5 – 10.0	408.23	406	406	232.15	231.6
10.0 – 50.0	1830.41	1838.5	1838	1186.44	1178
50.0 – 110.0	1795	1815	1838.1	868.34	879

*Normalized over this interval.

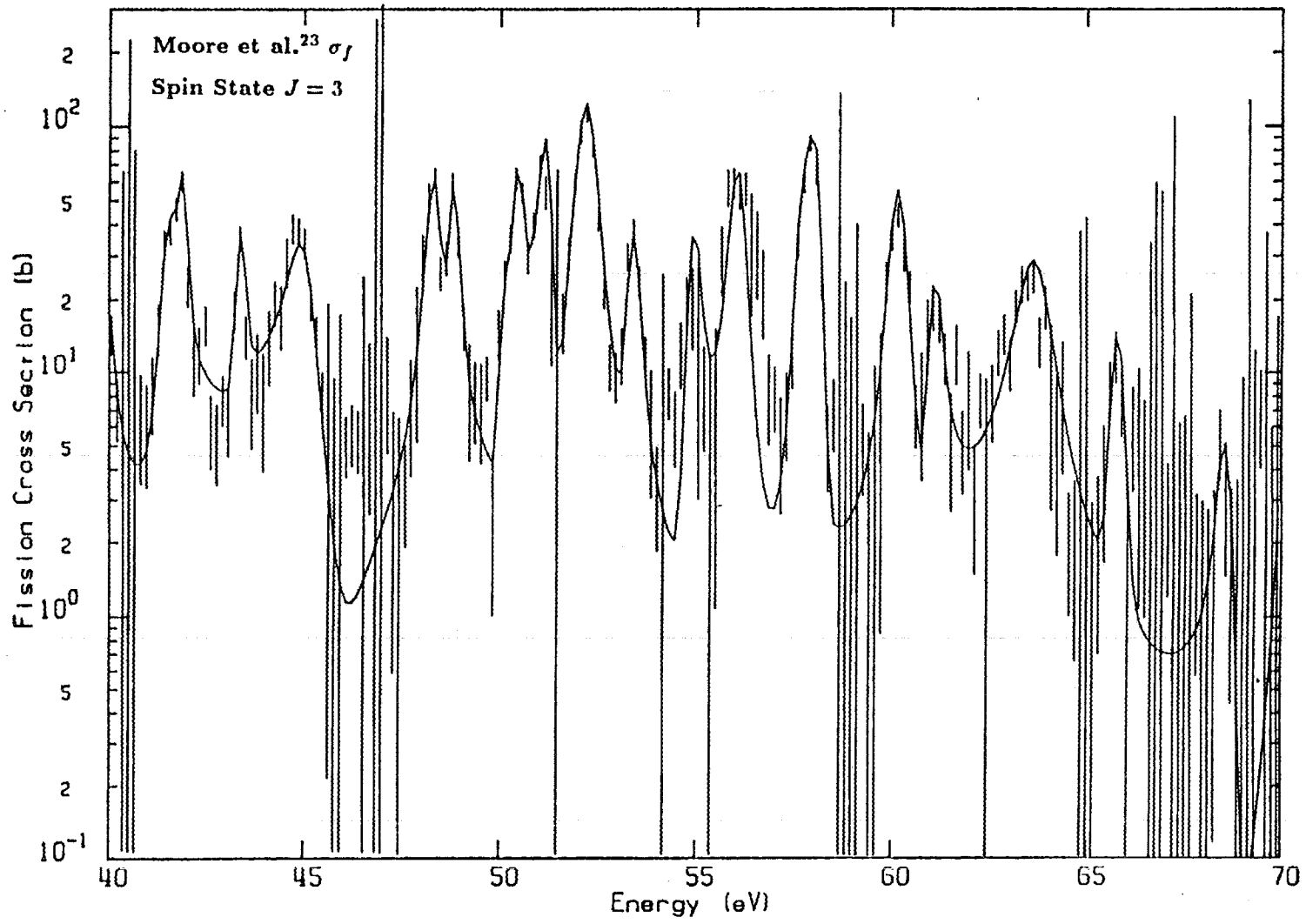


Fig. 5-10. Comparison of the spin separated fission cross-section data of Moore et al.²³ with calculations using the resonance parameters.

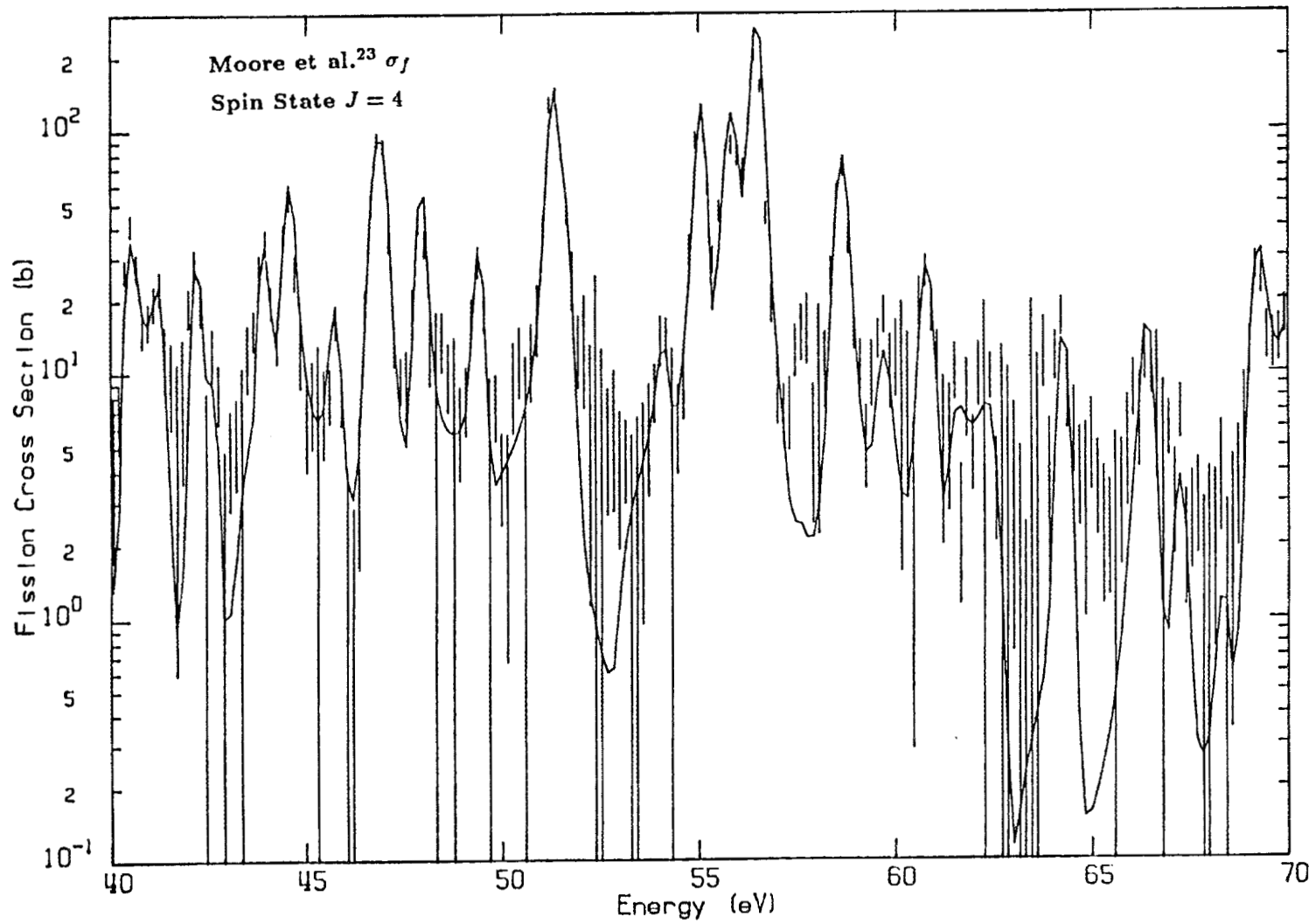


Fig. 5-11. Comparison of the spin separated fission cross-section data of Moore et al.²³ with calculations using the resonance parameters.

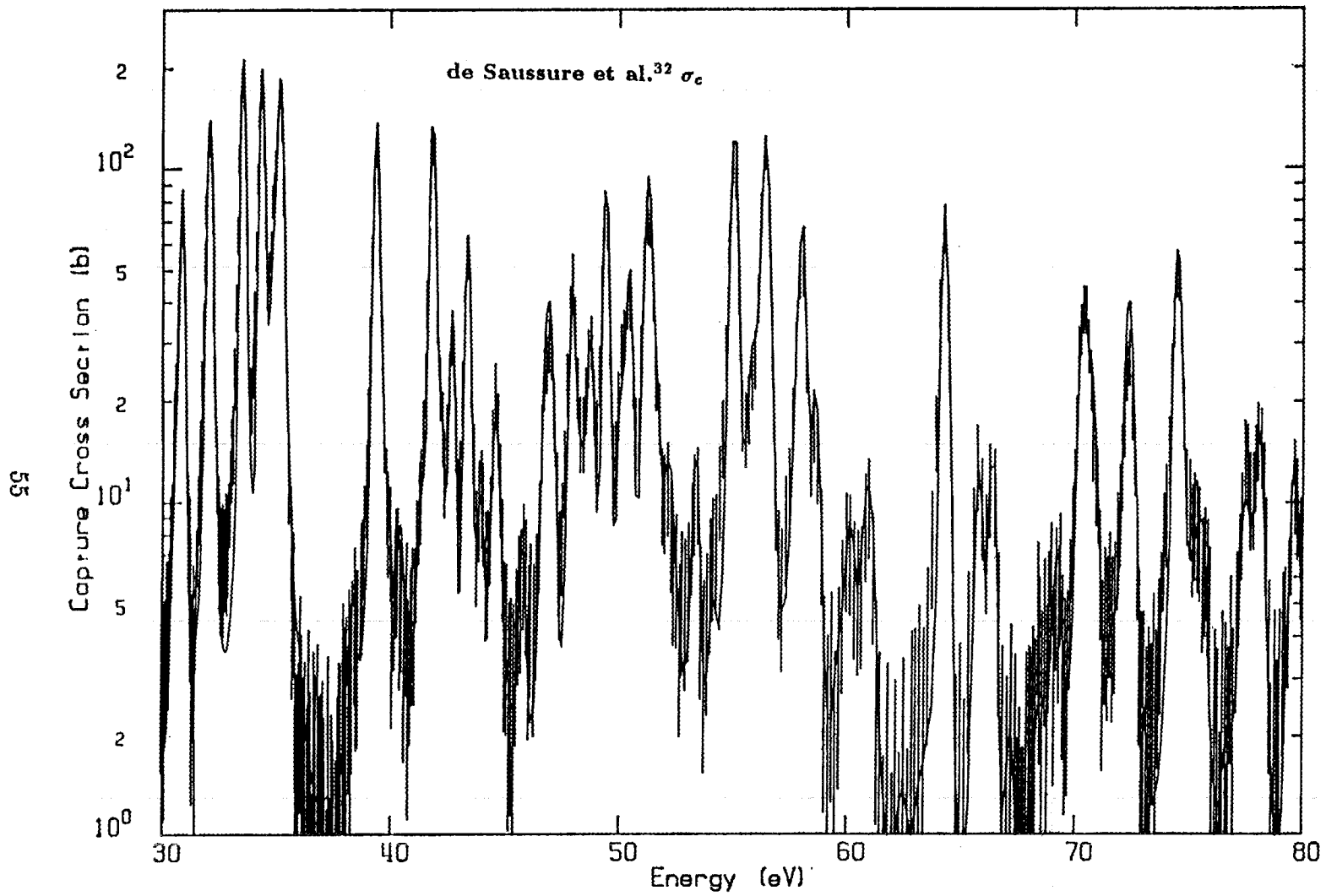


Fig. 5-12. Comparison of the capture cross-section data of de Saussure et al.³² with calculations using the resonance parameters.

Figures 5-13 to 5-16 show comparisons of the total cross-section data of Harvey et al., fission cross-section data of Weston and Todd,²⁷ and capture cross-section data of de Saussure et al. with calculations using the resonance parameters from 100 eV to 500 eV. For clarity of display, the total and capture cross-section data were displaced by one decade upward and two decades downward, respectively. Table 5-3 shows a comparison of the cross section averaged in intervals of 100 eV with the ENDF/B-V and an evaluation proposed by Carlson et al. The good agreement between the calculations and the experimental data, as shown in Fig. 5-13 to 5-16, will allow the direct computation of self-shielding factors by processing the cross section in these energy ranges. Discussion of this subject is given in Section 5.2.

Table 5-3. Comparison of average fission cross sections (b)

Energy interval (eV)	This evaluation	ENDF/B-V	Proposed by Carlson et al. ^a
100-200	20.58	20.71	21.14 ± 0.09
200-300	20.52	20.21	20.67 ± 0.10
300-400	13.02	12.90	13.14 ± 0.07
400-500	13.39	13.46	13.79 ± 0.07

^aThese values were obtained by the ENDF/B-VI Standards Committee.³⁸ They are not proposed as standards, and the uncertainties are still tentative.

Table 5-4 shows the results of fission and capture resonance integrals evaluated with the resonance parameters and from ENDF/B-V and compared to values obtained from integral measurements. Above 500 eV, the resonance integral values of ENDF/B-V (numbers indicated in parenthesis in the table) were taken since no resonance parameters were obtained above that range. The value of the fission resonance integral obtained in our analysis is 280.93 eV compared to 281.92 for

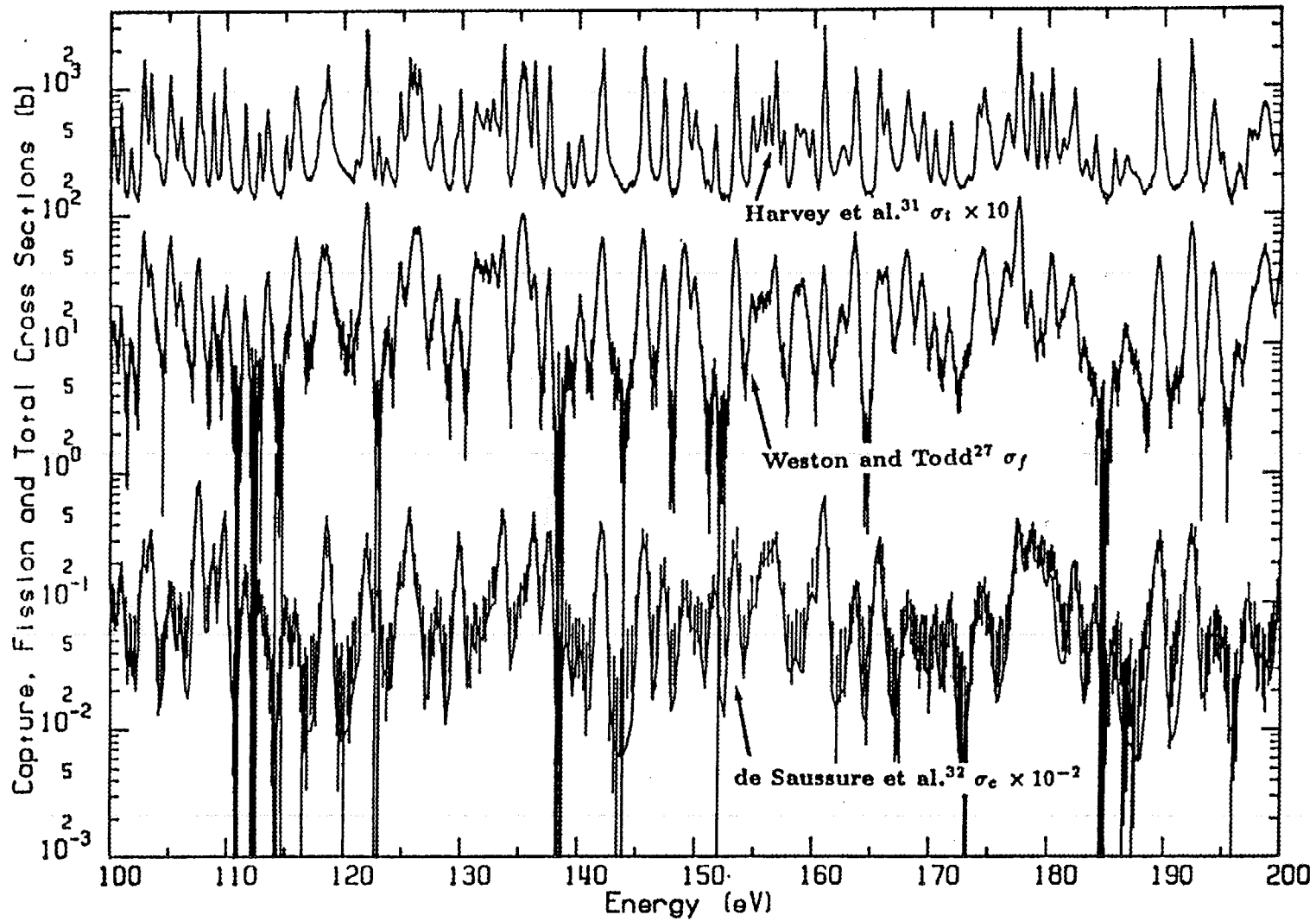


Fig. 5-13. Comparison of the total cross section of Harvey et al.,³¹ fission cross section of Weston and Todd,²⁷ and capture cross section of de Saussure et al.³² with calculations using the resonance parameters.

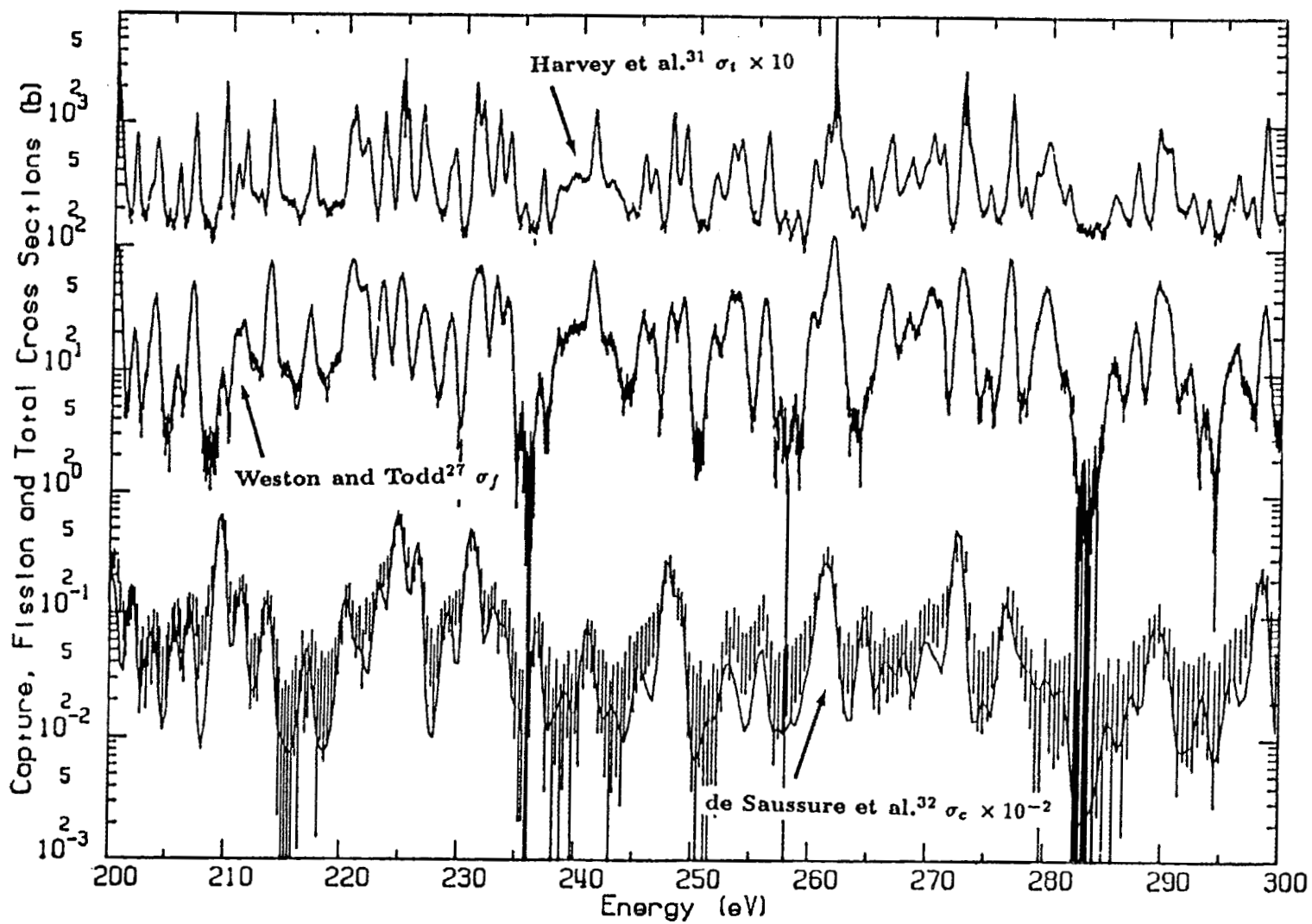


Fig. 5-14. Comparison of the total cross section of Harvey et al.,³¹ fission cross section of Weston and Todd,²⁷ and capture cross section of de Saussure et al.³² with calculations using the resonance parameters.

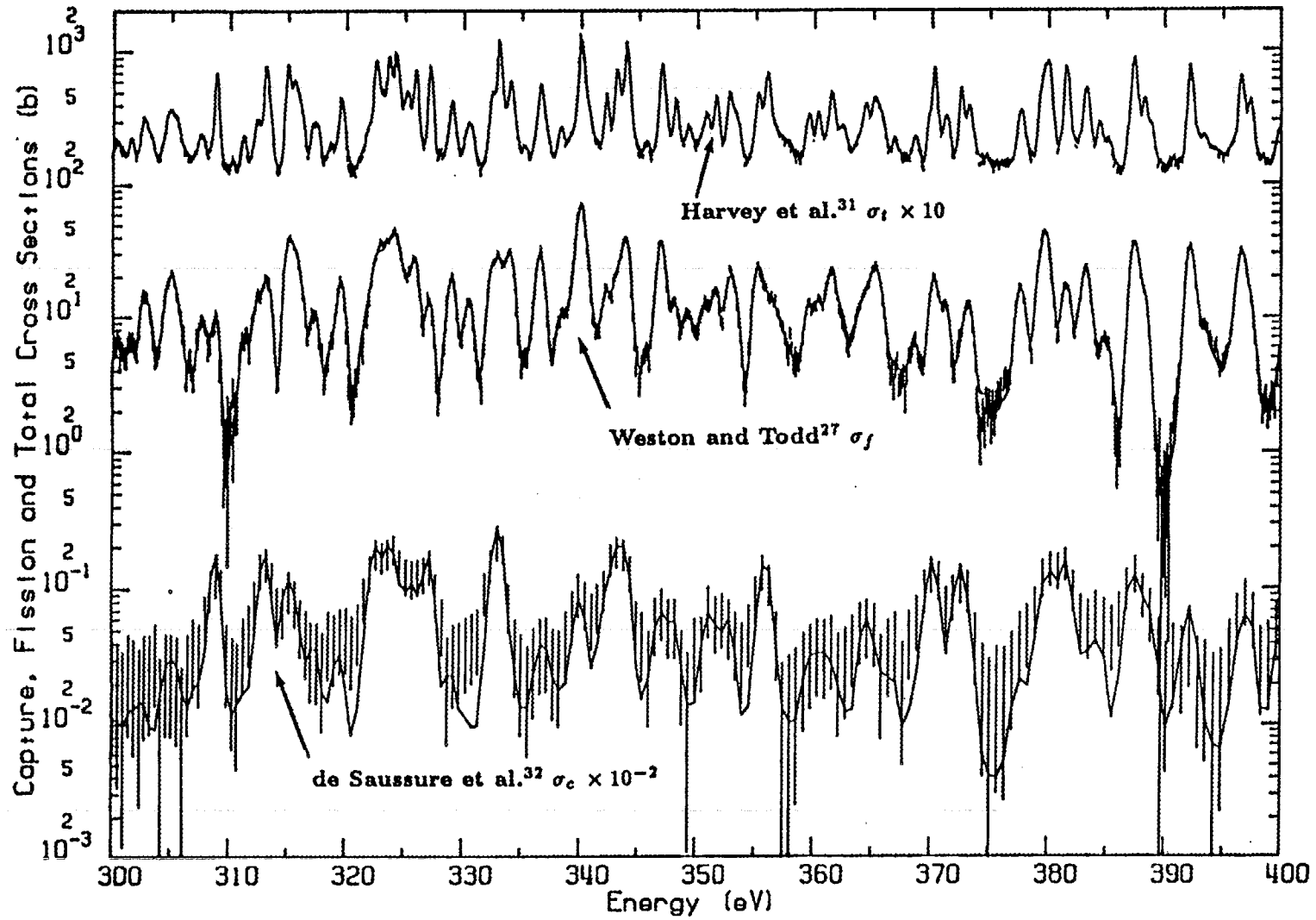


Fig. 5-15. Comparison of the total cross section of Harvey et al.,³¹ fission cross section of Weston and Todd,²⁷ and capture cross section of de Saussure et al.³² with calculations using the resonance parameters.

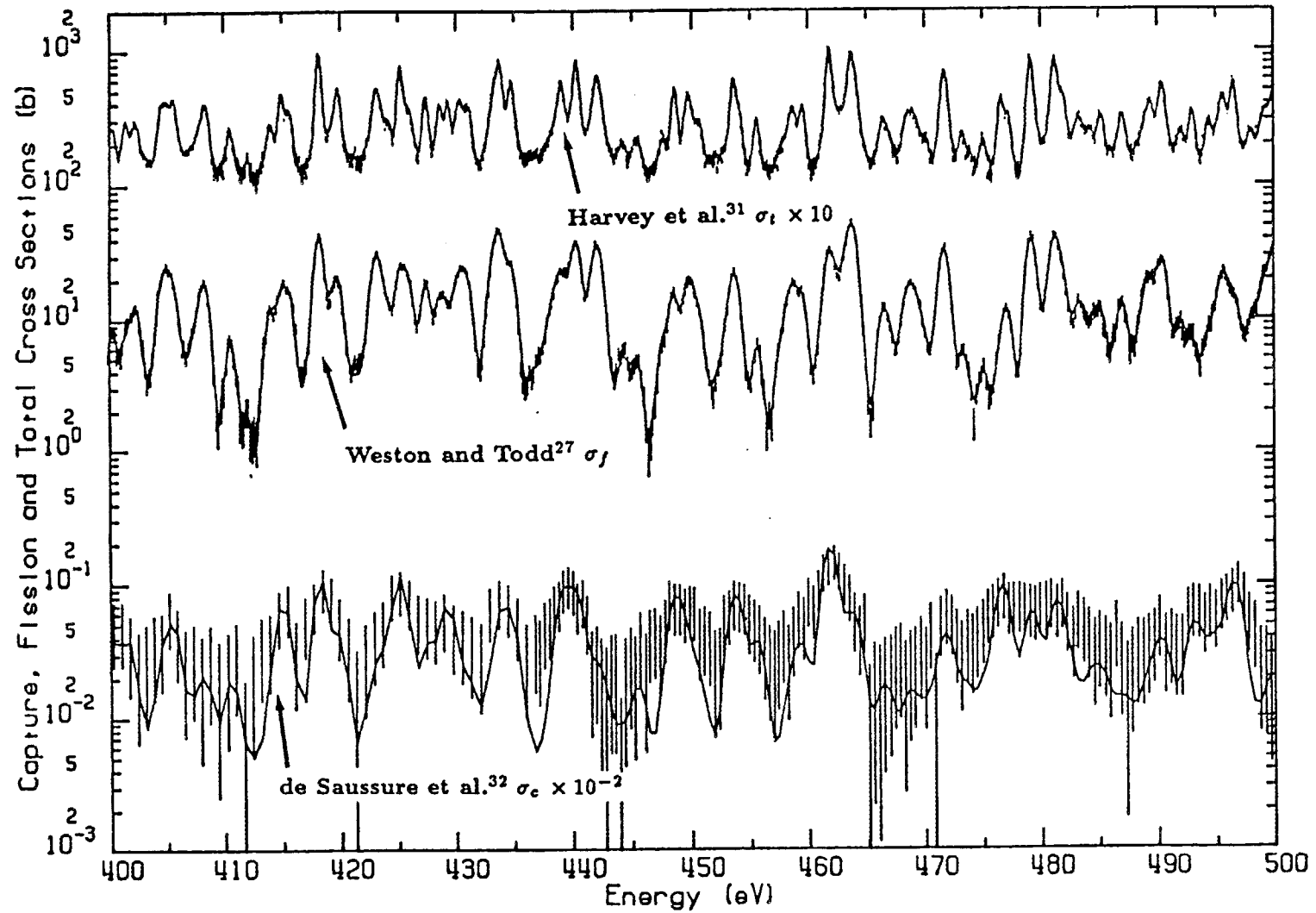


Fig. 5-16. Comparison of the total cross section of Harvey et al.,³¹ fission cross section of Weston and Todd,²⁷ and capture cross section of de Saussure et al.³² with calculations using the resonance parameters.

ENDF/B-V and to the value of 274 ± 5 obtained from integral measurements.³⁹ The ratio of the capture resonance integral to the fission resonance integral is 0.484 compared to 0.493 for ENDF/B-V and 0.513 ± 0.015 obtained from integral measurements.³⁹ At present, we do not understand the discrepancy in the ratio of the capture to the fission resonance integrals.

Table 5-4. Comparison of fission and capture resonance integrals (b)

Energy interval (eV)	Fission		Capture	
	This evaluation	ENDF/B-V	This evaluation	ENDF/B-V
0.5- 5	85.86	85.27	25.67	24.66
5- 50	110.12	111.68	77.07	78.49
50- 110	25.71	25.74	11.83	11.87
110- 300	20.92	20.93	8.77	10.67
300- 500	6.75	6.73	2.35	2.95
500 eV-20 MeV	(31.57)	31.57	(10.33)	10.33
0.5 eV-20 MeV	280.93	281.92	136.02	138.97

5.1 DISTRIBUTION OF THE RESONANCE PARAMETERS

Resonance parameters obtained from a multilevel R -matrix analysis of a consistent set of neutron cross sections are expected to satisfy a set of statistical properties arising from general properties of the nuclear Hamiltonian.¹⁰ A great deal of knowledge on the structure of the nucleus may be derived by examining the statistical properties of the nuclear resonance parameters. The purpose here is to present the results of the statistical distribution of the resonance parameters by graphical and tabular comparisons with the theory. In the graphical form, the results of the analysis will be given as histograms in which the dashed lines are the

experimental results and the solid lines represent the theory. The values obtained by averaging each quantity from 0 to 500 eV will be tabulated.

In Chapter II a brief review of the statistical theory was given, in which the χ^2 -distribution law for the level widths and the Wigner distribution law for the nearest energy level spacing distribution were introduced.

Figure 5-17 shows a comparison of the histograms of the normalized reduced neutron width distribution with the theoretical Porter-Thomas distribution which is a χ^2 -distribution with one degree of freedom. The comparison is shown for $J = 3$ and $J = 4$. The second moments calculated from the distribution of the reduced neutron widths are 2.71 ± 0.43 and 3.04 ± 0.34 for the spin states $J = 3$ and $J = 4$, respectively, and agree with the value of 3 for the theoretical Porter-Thomas distribution.

Figure 5-18 shows a comparison of the histograms of the fission-width distributions calculated with the resonance parameters for the two spin states $J = 3$ and $J = 4$, respectively, with a χ^2 -distribution with two degrees of freedom which is an exponential distribution. The experimental data do not allow for partitioning unambiguously the fission cross section into several channel components. Therefore, no good model is available with which to compare the observed distribution of fission widths. Figure 5-18 suggests that the distribution of total fission widths for each spin state is about consistent with a χ^2 -distribution with two degrees of freedom. A more detailed discussion of this topic has been presented by Moore et al.⁴⁰

In Fig. 5-19 we show histograms of the nearest neighbor-spacing distribution for each spin state $J = 3$ and $J = 4$ compared to a Wigner distribution. The second moments calculated from the observed spacings are 1.271 ± 0.067 and 1.210 ± 0.049

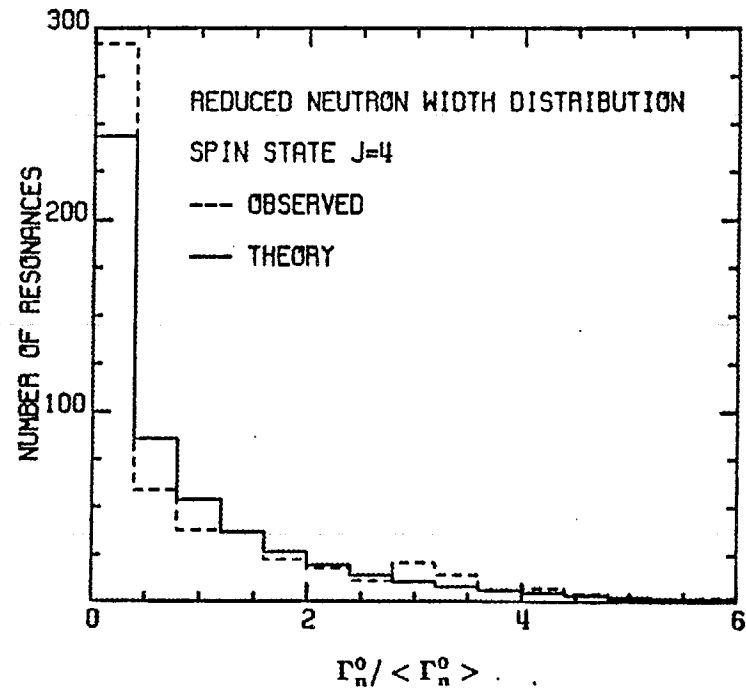
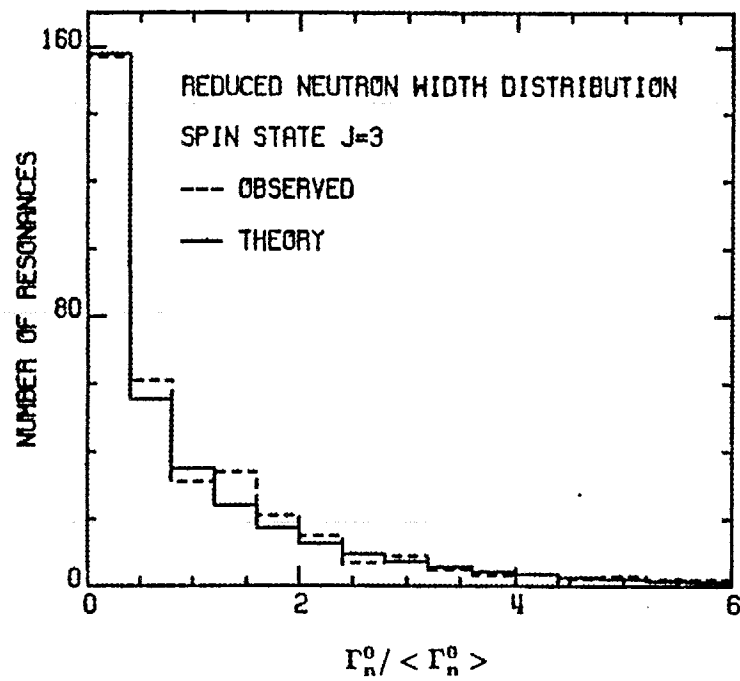


Fig. 5-17. Reduced neutron-width distributions compared to Porter-Thomas distributions.

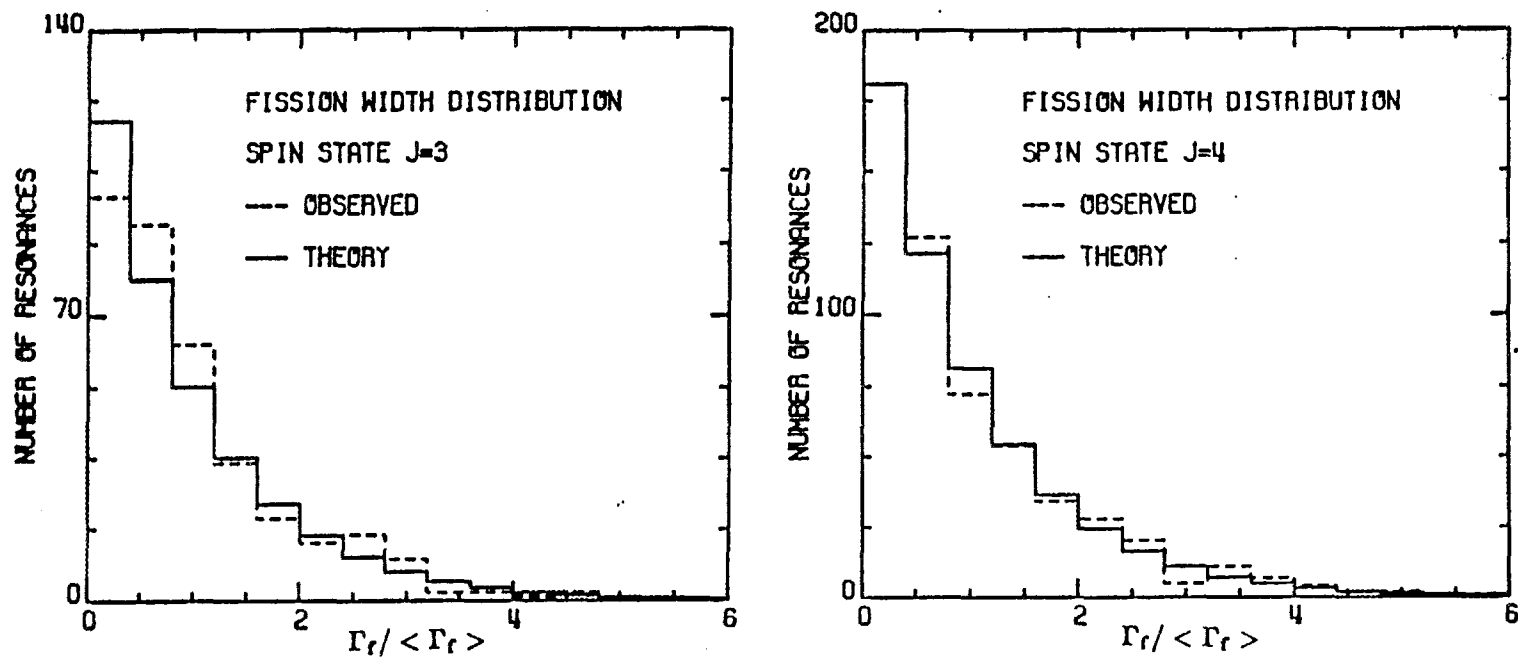


Fig. 5-18. Fission-width distributions compared to χ^2 distributions with two degrees of freedom.

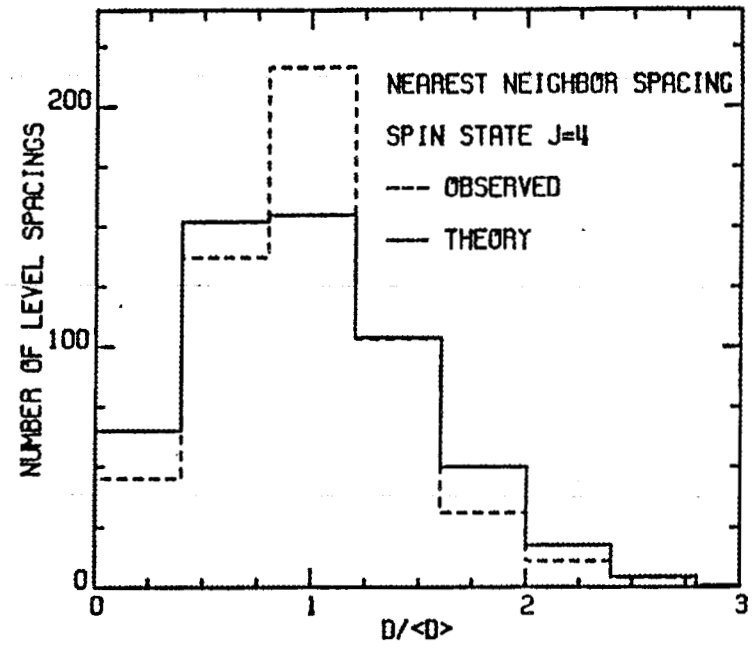
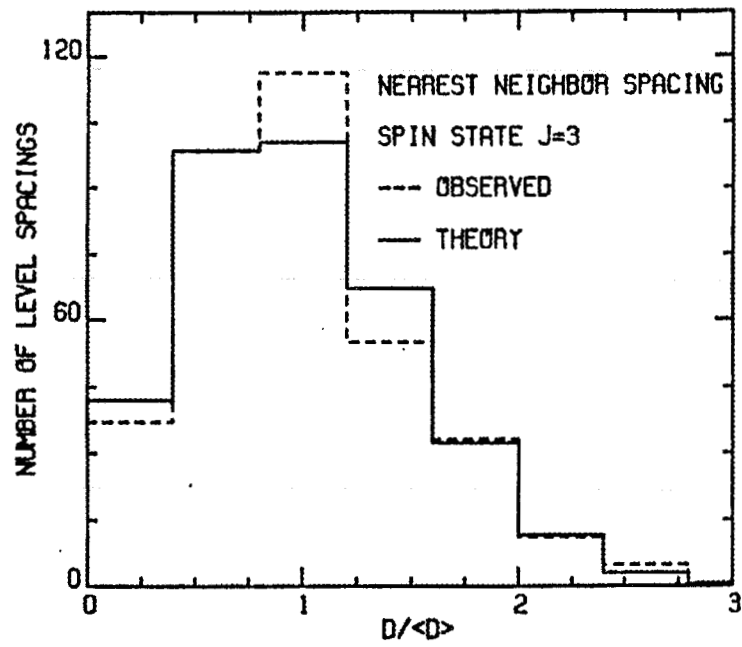


Fig. 5-19. Nearest neighbor-spacing distributions compared to Wigner distributions.

for the spin state $J = 3$ and $J = 4$. The second moment calculated from a Wigner distribution is 1.273.

Figure 5-20 shows histograms of the cumulative number of observed levels versus energy for each spin state as well as the lines fitted to these histograms. The steps of the histograms cannot be seen because of the scale. In a large scale the picture would resemble that indicated in the oval. The result indicated in Fig. 5-20 follows from the use of the Δ_3 -statistics technique. As is known, a crucial step in resonance analysis is to develop an appropriate spin state level-assignment procedure. The technique used consisted of combining the high-energy resolution data, spin-separated fission cross-section data, and the Δ_3 -statistics. For low energy, the identification of the resonances was made by the high-energy resolution data of Harvey et al. and their spin assigned according to the spin-separated fission cross-section data of Moore et al. This procedure was repeated up to approximately 100 eV where resonances can be experimentally resolved. The linear behavior of the cumulative sum of levels, following the Δ_3 -statistics, below 100 eV was extrapolated up to 500 eV. Above 100 eV, since resonances can not be fully resolved, resonances added at each spin state were tested with the Δ_3 -statistics and simultaneously fitted to the experimental measurements. The procedure was repeated up to 500 eV.

The results shown in Table 5-5 are the average values of the observed ^{235}U resonance parameter for each spin state and the results of the Δ_3 -statistics test. The average values of the reduced neutron widths and fission widths correspond to the histograms in Figs. 5-17 and 5-18, respectively, and the average level spacings to Fig. 5-20. The s -wave strength function, defined as the ratio between the average reduced neutron width and the average level spacings, is also given in Table 5-5.

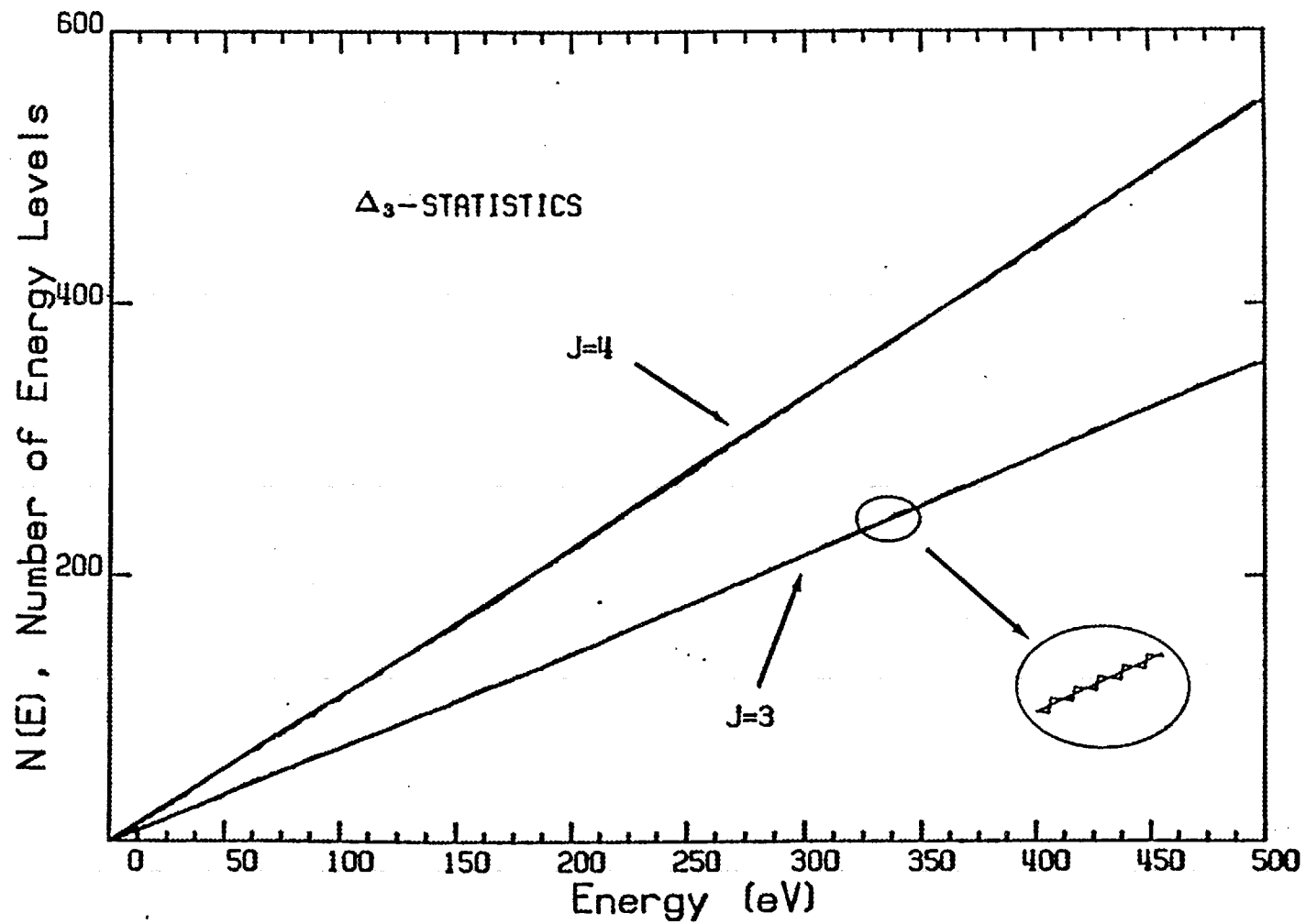


Fig. 5-20. Cumulative number of energy levels vs. energy. The steps of the histograms can not be seen in that scale.

Table 5-5. Average value of observed ^{235}U resonance parameters up to 500 eV

	$J = 3$	$J = 4$
Level spacing (eV)	1.396 ± 0.003	0.907 ± 0.002
Reduced neutron width (meV)	0.124 ± 0.075	0.092 ± 0.060
s -wave strength function ($\times 10^4$)	0.892 ± 0.067	1.013 ± 0.060
Fission width (meV)	256.2	225.8
Capture width (meV)	36	36
Observed Δ_3	0.53	0.68
Expected Δ_3	0.59 ± 0.11	0.63 ± 0.11

5.2 COMPARISON OF THE RESOLVED AND UNRESOLVED FORMALISMS

The resonance analysis performed in this work has extended the resolved resonance region from the previous ENDF/B-V limit of 82 eV up to the unprecedented upper limit of 500 eV. Hence, it now becomes feasible to perform a detailed comparison of the resolved and unresolved methodologies for the calculation of self-shielding factors. In the unresolved resonance range, the neutron cross-section representation is based on the statistical theory of neutron reactions, and the cross sections are specified by the average and distribution of resonance parameters.

The purpose here is to present a test of the validity of the ENDF/B formalism by comparing self-shielding factors computed with the ENDF/B unresolved formalism with values computed with the resolved resonance parameters of ^{235}U .

Self-shielding factors for constant flux can be obtained as the ratio of two integrals over the energy range of a group as

$$f_x^* = \frac{1}{\bar{\sigma}_{nx}} \frac{\int \frac{\sigma_{nx}(E)}{\sigma_t(E) + \sigma_0} dE}{\int \frac{dE}{\sigma_t(E) + \sigma_0}} \quad (5-1)$$

where $\sigma_{nx}(E)$ and $\sigma_t(E)$ are the Doppler-broadened energy dependent partial and total cross sections computed with the evaluated resonance parameters, and σ_0 is the dilution cross section.

The unresolved resonance formalism for the self-shielding factors corresponding to Eq. (5-1) are obtained by the Bondarenko⁴¹ formula

$$f_x = \frac{1}{\langle \sigma_{nx} \rangle} \frac{\left\langle \frac{\sigma_{nx}}{\sigma_t + \sigma_0} \right\rangle}{\left\langle \frac{1}{\sigma_t + \sigma_0} \right\rangle} \quad (5-2)$$

where the brackets indicate an average over the appropriate statistical distributions as specified in ENDF/B-V.

Fission and capture self-shielding factors were computed with both formalisms as a function of temperature and dilution. Results of this comparison are shown in Table 5-6. The first two columns of the table give the neutron energy boundaries of the group; the next three columns give the fission self-shielding factors, as computed with Eqs. (5-1) and (5-2) above, and their ratio; the last three columns give corresponding capture self-shielding factors. All self-shielding factors given in the table are for a temperature of 300 K. A comparison is shown for four energy groups and three typical dilutions.

From the table it can be seen that for large dilutions ($\sigma_0 = 1000$ b) the self-shielding factors computed with the resolved or unresolved formalisms are consistent to within 1% or better; however, for smaller dilutions the two methods give results that, over groups 100 eV wide, may differ by as much as 7%, as is the case for f_γ for the 200-300 eV group.

Table 5-6. Comparison of fission and capture selfshielding factors.

Group Boundaries (eV)	f_f	f_f^*	f_f^*/f_f	f_γ	f_γ^*	f_γ^*/f_γ
Dilution 50 b						
100–200	.795	.787	.99	.757	.734	.97
200–300	.799	.803	1.01	.713	.763	1.07
300–400	.874	.882	1.01	.839	.857	1.02
400–500	.893	.937	1.05	.881	.909	1.03
Dilution 100 b						
100–200	.855	.855	1.00	.826	.814	.99
200–300	.859	.881	1.03	.788	.847	1.07
300–400	.917	.929	1.01	.893	.917	1.03
400–500	.930	.964	1.04	.922	.945	1.02
Dilution 1000 b						
100–200	.976	.975	1.00	.970	.967	.99
200–300	.976	.982	1.01	.961	.975	1.01
300–400	.988	.990	1.00	.985	.987	1.00
400–500	.990	.996	1.01	.989	.993	1.00

Such differences may have been expected for the following reasons: (1) the unresolved resonance parameters are constrained to reproduce the evaluated average cross sections at selected energies, but these constraints are not sufficient to determine a unique set of parameters; (2) the group-averaged self-shielding factors are very sensitive to the statistical distributions of the resonance parameters, and these distributions may differ appreciably over the group from the distributions specified in the ENDF/B-V evaluation; and (3) the unresolved resonance approach

is based on the Breit-Wigner single-level formalism which cannot represent correctly the level-level interferences in the fission cross section.

The conclusion is that the ENDF/B-V unresolved resonance formalism is adequate to compute the resonance self-shielding in ^{235}U in the range 100 to 500 eV for large dilutions ($\sigma_0 = 1000$ b). For smaller dilutions, the formalism may yield values of the self-shielding factors in error by a few percent. For most commercial reactors fueled with low enrichment uranium, the self-shielding in ^{235}U is unimportant since the nuclear Doppler effect is dominated by the ^{238}U resonance absorption. However, for research reactors fueled with highly enriched ^{235}U , such as the Advanced Neutron Source (ANS)⁴² now being designed at ORNL, the self-shielding factors and their variations with temperature are important core parameters. For such applications, it is preferable to represent evaluated neutron cross sections with resolved resonances for all energies where self-shielding is not negligible.

CHAPTER VI

CONCLUSIONS AND RECOMMENDATIONS

The R -matrix resonance analysis of the recently available high-resolution ^{235}U neutron-induced cross sections has yielded resonance parameters for 912 s -wave resonances in an energy range up to 500 eV. In performing this analysis, the use of the Δ_3 -statistics has proven to be an invaluable methodology for the difficult task of resonance spin assignments in the neutron energy range above 100 eV where the resonances cannot be fully resolved.

The use of the Bayesian approach, implemented in the program SAMMY, has been a powerful tool for the renormalization and background corrections of cross section data sets, as well as for accounting for other experimental uncertainties such as those associated with sample thickness determination.

The method for resonance Doppler-broadening, developed in this dissertation, was shown to be more accurate than the method based on the traditional Voigt profiles, especially in the low-neutron energy range, and has been adopted for use in the general utility R -matrix program SAMMY.

The present resonance analysis up to 500 eV has provided an unprecedented large, almost pure (i.e., not contaminated by p -wave resonances), statistical sample of ^{235}U resonance parameters. On this basis, a statistically meaningful analysis of resonance-parameter distributions has been made possible. It has been concluded with good statistical precision that both the neutron widths and nearest neighbor spacing distributions follow the Porter-Thomas and Wigner distributions, respectively. For the fission widths, the present analysis shows that the distribution of the total fission widths for each spin state follows a χ^2 distribution with two

degrees of freedom, which is consistent with the presence of two fully open fission channels.

The comparison between resolved and unresolved resonance formalisms for the calculation of self-shielding factors has shown that the use of the latter formalism at low dilutions may yield values for the self-shielding factors in error by a few percent. Since the self-shielding factors and their temperature dependence are important for research reactors fueled with highly enriched ^{235}U , such as the Advanced Neutron Source (ANS) reactor, one concludes that for such an application it is preferable to represent evaluated neutron cross sections with resolved resonances.

The conversion of the Reich-Moore R -matrix parameter sets into Adler-Adler and multipole-expansion parameter sets provides flexible and accurate alternatives for the representation of the ^{235}U neutron induced cross sections. Although the multipole-expansion is completely rigorous in its treatment of energy dependence of the neutron widths, the present work substantiates the conclusion that the simpler Adler-Adler representation, acceptable in the ENDF/B formats and procedures, yields a reasonably accurate representation of the fissile isotopes neutron cross sections for nuclear reactor design.

We recommend, for future work, that the integral measurements of self-shielded rates in ^{235}U of Bramblett and Czirr,⁴³ and Czirr⁴⁴ which serves as benchmarks for evaluations of the ^{235}U differential neutron cross sections, should be compared with integral calculations using the present set of resonance parameters. Also, the use of the present resonance analysis methodology should provide an extension of the resolved resonance range in ^{235}U up to 2 keV.

The application of the Δ_3 -statistics for resonance spin assignments provides the necessary algorithm for new improved resonance analysis of the ^{239}Pu and

^{241}Pu isotopes, since high-resolution measurements of their cross sections are now available.

The use of the Bayesian approach, which incorporates data uncertainties and experimental conditions together with the Δ_3 -statistics for spin assignments, is highly recommended for any future work on the process of resonance analysis.

LIST OF REFERENCES

LIST OF REFERENCES

1. National Nuclear Data Center, Brookhaven National Laboratory Associated Universities, INC., Upton, Long Island, New York 11973.
2. "CSISRS: Cross-Section Information Standard Retrieval System," Brookhaven National Laboratory.
3. "CINDA: The Index to Literature and Computer Files on Microscopic Neutron Data," International Atomic Energy Agency (1987).
4. F. C. Maienschein, *Energia Nuclear*, **79**, 533 (1972). English translation in ORNL-TM-3833 (1972).
5. N. M. Larson, ORNL/TM-9710/R1 (1985) and ORNL/TM-9179/R2 (1989); N. M. Larson and F. G. Perey, Intern. Conf. Nuclear Data for Science and Technology, May 30-June 3, 1988, Mito, Japan (1988).
6. E. P. Wigner and L. Eisenbud, *Phys. Rev.* **72** (1947) 29, E. P. Wigner, *J. Am. Phys. Soc.* **17** (1949) 99.
7. A. M. Lane and R. G. Thomas, *Rev. Mod. Phys.* **30** (1958) 257.
8. J. E. Lynn, *Neutron Resonance Reactions*, Oxford, 1968.
9. C. W. Reich and M. S. Moore, *Phys. Rev.* **111** (1958) 929.
10. C. E. Porter and R. G. Thomas, *Phys. Rev.* **104** (1956) 483.
11. A. Bohr, *Proc. Conf. on Peaceful Uses of Atomic Energy, Geneva, 1955*, Vol. 2, p. 151.
12. D. B. Adler and F. T. Adler, *Proceedings of the Conference on Breeding, Economics, and Safety in Large Fast Power Reactors*, ANL-6792, Oct. 7-10, 1963.

13. G. de Saussure and R. B. Perez, *POLLA, A FORTRAN Program to Convert R-Matrix-Type Multilevel Resonance Parameters into Equivalent Kapur-Peierls-Type Parameters*, ORNL-2599, Oak Ridge National Laboratory (1969).
14. R. N. Hwang, *Nucl. Sci. and Eng.* **96** (1987) 192.
15. E. P. Wigner, Conf. on Neutron Physics by Time-of-Flight, Gatlinburg, Tennessee, 1956, Report ORNL-2309 (1957) p. 59.
16. M. L. Mehta, *Nucl. Phys.* **18** (1960) 395.
17. F. J. Dyson and M. L. Mehta, *J. Mathe. Phys.* **4** (1963) 701.
18. W. E. Lamb, *Phys. Rev.* **55** (1939) 190.
19. L. Dresner, *Resonance Absorption in Nuclear Reactors*, Pergamon Press, New York (1960).
20. A. W. Solbrig, Jr., *Nucl. Sci. Eng.*, **10** (1961) 167.
21. T. M. Shih, *Numerical Heat Transfer*, Hemisphere Publishing Company, Washington, D. C. (1984).
22. G. D. James and G. De Saussure in *Nuclear Fission and Neutron-Induced Fission Cross-Sections*, Editor A. Michaudon, Pergamon Press 1981, also F. H. Fröhner, *Applied Neutron Resonance Theory*, KfK-2669, Kernforschungszentrum Karlsruhe, pg. 30 (1978).
23. M. S. Moore, J. D. Moses, G. A. Keyworth, J. W. T. Dabbs, N. W. Hill, *Phys. Rev.*, **C18**, 3, 1328 (1978).
24. C. Wagemans et al., "Subthermal Fission Cross-Section Measurements for ^{233}U , ^{235}U , and ^{239}U ," presented at Int. Conf. Nuclear Data for Science and Technology, Mito, Japan (1988).

25. J. Blons, *Nucl. Sci. Eng.* **51**, 130 (1973).
26. L. W. Weston and J. H. Todd, *Nucl. Sci. Eng.* **88**, 567 (1973).
27. L. W. Weston, private communication.
28. R. Gwin, R. R. Spencer, R. W. Ingle, J. H. Todd, S. W. Scoles, *Nucl. Sci. Eng.* **88**, 37 (1984).
29. R. C. Schrack, "Measurement of the $^{235}\text{U}(n, f)$ Reaction from Thermal to 1 KeV," paper presented at the Internat. Conf. Nuclear Data for Science and Technology, May 30-June 3, 1988, Mito, Japan (1988).
30. R. R. Spencer, J. A. Harvey, N. W. Hill, L. W. Weston, *Nucl. Sci. Eng.* **96**, 318(1987).
31. J. A. Harvey, N. W. Hill, F. G. Perey, G. L. Tweed and L. Leal, "High-Resolution Neutron Transmission Measurements on ^{235}U , ^{238}U , and ^{239}Pu ," paper presented at the Internat. Conf. Nuclear Data for Science and Technology, May 30-June 3, 1988, Mito, Japan (1988).
32. G. de Saussure, R. Gwin, L. W. Weston, R. W. Ingle, *Simultaneous Measurements of Neutron Fission Capture Cross Sections for ^{235}U for Incident Neutron Energies from 0.4 eV to 3 keV*, ORNL-TM-1804, Oak Ridge National Laboratory (1967).
33. C. Coceva, R. Simonini, and D. K. Olsen, "Calculation of the ORELA Neutron Moderator Spectrum and Resolution Function," *Nucl. Inst. and Meth.* **211**, 459 (1983).
34. F. G. Perey, J. A. Harvey, and N. W. Hill, "The ^{56}Fe 1.15-Kev Resonance Parameters from Transmission Measurements at ORELA", communication to the 1.15-Kev NEANDC Task Force, March 1983, and private communication.

35. S. F. Mughabghab, *Neutron Resonance Parameters and Thermal Cross Sections*, 1 Brookhaven National Laboratory (1984).
36. *American Institute of Physics Handbook* (Third Edition, 1972) pg. 4-31
37. J. T. Reynolds, *Reich and Moore Multilevel Analysis of ^{235}U Neutron Cross Sections*, KAPL-M-7396, Knolls Atomic Power Laboratory (October 1975).
38. A. Carlson et al., National Bureau of Standards, "Results of the ENDF/B-VI Standards Evaluation," August 1987.
39. J. Hardy, *^{235}U Resonance Fission Integral and Alpha Based on Integral Measurements*, ENDF-300, Sec. B.1, Brookhaven National Laboratory (1979).
40. M. S. Moore, L. C. Leal, G. de Saussure, R. B. Perez and N. M. Larson, "Resonance Structure in the Fission of ($^{235}\text{U}+\text{n}$)," *Nuclear Physics*, **A502** (1989) 443c-452c.
41. I. I. Bondarenko et al. *Group Constant for Nuclear Reactor Calculations*, Consultants Bureau, New York (1964).
42. F. C. Difilippo, R. M. Moon, W. R. Gambill, R. T. Prim, III and C. D. West, "An Intense Steady-State Neutron Source-The CNR Reactor," *Proc. Topl. Mtg. Reactor Physics and Safety, Saratoga Springs, New York, September 17-19, 1986*, NUREG/CP-0800, Vol. 2 p. 792, U. S. Nuclear Regulatory Commission (1986).
43. R. L. Bramblett and J. B. Czirr, *Nucl. Sci. Eng.* **35**, 350-357 (1969) .
44. J. B. Czirr, *Nucl. Sci. Eng.* **70**, 307-317 (1979).

APPENDICES

APPENDIX A

RELATIONSHIP BETWEEN MATRICES U, R, AND A

A.1 Relation between the collision matrix U and the matrix R

The penetration factor defined in Eq. (2-27) can be obtained as the imaginary part of the logarithmic derivative \mathbf{L} as

$$\mathbf{P} = \text{Im} \left(r \phi_{\text{out}}^{-1} \frac{d\phi_{\text{out}}}{dr} \right)_{r=a} . \quad (\text{A} - 1)$$

From Eq. (2-16) we obtain that $\mathbf{P} = \rho (\phi_{\text{in}} \phi_{\text{out}})^{-1}$ where $\rho = ka$.

Defining $\mathbf{\Omega} = \phi_{\text{in}}^{1/2} \phi_{\text{out}}^{-1/2}$, Eq. (2-26) can be written as

$$\mathbf{U} = \mathbf{\Omega} \mathbf{P}^{1/2} (\mathbf{I} - \mathbf{R} \mathbf{L}_0)^{-1} (\mathbf{I} - \mathbf{R} \bar{\mathbf{L}}_0) \mathbf{P}^{-1/2} \mathbf{\Omega} . \quad (\text{A} - 2)$$

Since \mathbf{S} and \mathbf{P} are real matrices, $\bar{\mathbf{L}}_0$ is given by $\bar{\mathbf{L}}_0 = \mathbf{L}_0 - 2i\mathbf{P}$ which leads to

$$\mathbf{U} = \mathbf{\Omega} \mathbf{P}^{1/2} (\mathbf{I} - \mathbf{R} \mathbf{L}_0)^{-1} (\mathbf{I} - \mathbf{R} \mathbf{L}_0 + 2i\mathbf{P}) \mathbf{P}^{-1/2} \mathbf{\Omega} , \quad (\text{A} - 3)$$

or

$$\mathbf{U} = \mathbf{\Omega} \left[\mathbf{I} + 2i\mathbf{P}^{1/2} (\mathbf{I} - \mathbf{R} \mathbf{L}_0)^{-1} \mathbf{P}^{1/2} \right] \mathbf{\Omega} , \quad (\text{A} - 4)$$

which is Eq. (2-30).

A.2 Relation between the channel and the level matrices

The \mathbf{R} matrix is defined as

$$\mathbf{R} = \sum_{\lambda} \frac{\gamma_{\lambda} \times \gamma_{\lambda}}{E_{\lambda} - E} , \quad (\text{A} - 5)$$

where $\gamma_{\lambda} \times \gamma_{\lambda}$ indicates the direct product between two vectors.

The expression $\mathbf{I} - \mathbf{RL} = \mathbf{1} - \sum_{\lambda} \frac{\gamma_{\lambda} \times \gamma_{\lambda}}{E_{\lambda} - E} \mathbf{L}$ can be written as

$$\mathbf{I} - \mathbf{RL} = \mathbf{1} - \sum_{\lambda} \frac{\gamma_{\lambda} \times \beta_{\lambda}}{E_{\lambda} - E} , \quad (\text{A} - 6)$$

where we have defined $\beta_{\lambda} = \mathbf{L}\gamma_{\lambda}$ and used the identity $\mathbf{Ax} + \mathbf{By} = \mathbf{A}(\mathbf{x} + \mathbf{y})\mathbf{B}^{\dagger}$ in which \mathbf{A} and \mathbf{B} are matrices, \mathbf{x} and \mathbf{y} are vectors, and \mathbf{L} is a symmetric matrix.

The form of Eq. (A-6) suggests the following relation

$$(\mathbf{I} - \mathbf{RL})^{-1} = \mathbf{1} + \sum_{\mu\nu} (\gamma_{\mu} \times \beta_{\nu}) \mathbf{A}_{\mu\nu} , \quad (\text{A} - 7)$$

with the indices μ and ν referring to energy levels.

Multiplying Eqs. (A-6) and (A-7) and using the identity $(\mathbf{x} \times \mathbf{y})(\mathbf{z} \times \mathbf{w}) = (\mathbf{y} \cdot \mathbf{z})(\mathbf{x} \times \mathbf{w})$, we obtain the following expression,

$$\sum_{\mu\nu} (\gamma_{\mu} \times \beta_{\nu}) \mathbf{A}_{\mu\nu} - \sum_{\lambda} \frac{\gamma_{\lambda} \times \beta_{\lambda}}{E_{\lambda} - E} - \sum_{\lambda\mu\nu} \frac{\gamma_{\lambda} \times \beta_{\nu}}{E_{\lambda} - E} (\beta_{\lambda} \cdot \gamma_{\mu}) \mathbf{A}_{\mu\nu} = \mathbf{0} . \quad (\text{A} - 8)$$

Factorizing the term $\gamma_{\lambda} \times \beta_{\nu}$ in the equation above, we find

$$\sum_{\lambda\nu} (\gamma_{\lambda} \times \beta_{\nu}) \left[\mathbf{A}_{\lambda\nu} - \frac{\delta_{\lambda\nu}}{E_{\lambda} - E} - \sum_{\mu} \frac{(\beta_{\lambda} \cdot \gamma_{\mu})}{E_{\lambda} - E} \mathbf{A}_{\mu\nu} \right] = \mathbf{0} , \quad (\text{A} - 9)$$

which leads to Eq. (2-32).

The evaluation of the matrix $(\mathbf{I} - \mathbf{RL})^{-1}\mathbf{R}$ is obtained by combining Eqs. (A-6) and (A-7) which gives

$$(\mathbf{I} - \mathbf{RL})^{-1}\mathbf{R} = \sum_{\lambda} \left[\frac{\gamma_{\lambda} \times \gamma_{\lambda}}{E_{\lambda} - E} + \frac{1}{E_{\lambda} - E} \sum_{\mu} (\gamma_{\mu} \times \gamma_{\lambda}) \sum_{\nu} (\beta_{\nu} \cdot \gamma_{\lambda}) \mathbf{A}_{\mu\nu} \right] . \quad (\text{A} - 10)$$

Using Eq. (2-32) as $\sum_{\nu} (\beta_{\nu} \cdot \gamma_{\lambda}) \mathbf{A}_{\mu\nu} = -\delta_{\lambda\mu} + (E_{\lambda} - E) \mathbf{A}_{\lambda\mu}$ in the previous equation, we get

$$(\mathbf{I} - \mathbf{RL})^{-1}\mathbf{R} = \sum_{\mu\lambda} (\gamma_{\mu} \times \gamma_{\lambda}) \mathbf{A}_{\mu\lambda} . \quad (\text{A} - 11)$$

APPENDIX B

REICH-MOORE AND ADLER-ADLER NEUTRON CROSS-SECTION FORMALISM

B.1 Reich-Moore Formalism

Total Cross Section

$$\sigma_{nT}^J = 2\pi\lambda^2 g \left[1 - \cos(2ka) \right] + 4\pi\lambda^2 g \operatorname{Re} \left[\rho_{nn} \exp(2ika) \right] . \quad (\text{B} - 1)$$

Absorption Cross Section

$$\sigma_{nA}^J = 4\pi\lambda^2 g \left[\operatorname{Re}(\rho_{nn}) - |\rho_{nn}|^2 \right] . \quad (\text{B} - 2)$$

Fission Cross Section

$$\sigma_{nF}^J = 4\pi\lambda^2 g \sum_c |\rho_{nc}|^2 , \quad (\text{B} - 3)$$

where

$$\rho_{nc} = \frac{\Delta \delta_{nc} - m_{nc}}{\Delta} , \quad (\text{B} - 4)$$

$$\Delta = |I - K| , \quad (\text{B} - 5)$$

$$m_{nc} = \Delta \left[(I - K)^{-1} \right]_{nc} , \quad (\text{B} - 6)$$

and

$$(I - K)_{cic} = \delta_{cic} - \frac{i}{2} \sum_{\lambda} \frac{(\Gamma_{\lambda c} \Gamma_{\lambda ci})^{1/2}}{E_{\lambda} - E - \frac{i}{2} \Gamma_{\lambda \gamma}} . \quad (\text{B} - 7)$$

The symbols appearing in the equations above are defined in the text.

B.2 Adler-Adler Formalism

Total Cross section

$$\sigma_{nT} = 2\pi\lambda^2 g \left[1 - \cos(2ka) \right] + \frac{1}{\sqrt{E}} \sum_{\lambda} \frac{\nu_{\lambda} G_{\lambda}^T + (\mu_{\lambda} - E) H_{\lambda}^T}{(\mu_{\lambda} - E) + \nu_{\lambda}^2}, \quad (\text{B} - 8)$$

Absorption Cross Section

$$\sigma_{nA} = \frac{1}{\sqrt{E}} \sum_{\lambda} \frac{\nu_{\lambda} G_{\lambda}^A + (\mu_{\lambda} - E) H_{\lambda}^A}{(\mu_{\lambda} - E) + \nu_{\lambda}^2}, \quad (\text{B} - 9)$$

Fission Cross Section

$$\sigma_{nF} = \frac{1}{\sqrt{E}} \sum_{\lambda} \frac{\nu_{\lambda} G_{\lambda}^F + (\mu_{\lambda} - E) H_{\lambda}^F}{(\mu_{\lambda} - E) + \nu_{\lambda}^2}, \quad (\text{B} - 10)$$

where

$$G_{\lambda}^T = \alpha_{\lambda} \cos(2ka) + \beta_{\lambda} \sin(2ka) \quad (\text{B} - 11)$$

and

$$H_{\lambda}^T = \beta_{\lambda} \cos(2ka) - \alpha_{\lambda} \sin(2ka). \quad (\text{B} - 12)$$

APPENDIX C
 RESONANCE PARAMETERS FOR THE THREE
 REPRESENTATIONS

Table C-1. Evaluated Reich-Moore resonance parameters

E (eV)	Γ_γ (meV)	Γ_n (meV)	Γ_{f1} (meV)	Γ_{f2} (meV)	J
-100.00	38.92	11.458	0.123	72.264	3
-90.00	37.00	2.422-3 ^a	56.114	-216.68	4
-4.2976	35.00	7.1641	318.98	-115.23	4
-3.4934	38.00	8.472-5 ^a	-6.753	12.973	3
-1.5043	37.87	8.520-5 ^a	-7.004	12.309	3
-0.41161	30.00	0.14875	-1.026	-155.26	3
-0.19428	35.22	5.045-4	198.76	-1.692	4
3.657-5 ^a	30.00	6.505-8 ^a	-0.526	0.964	4
0.28190	38.57	0.00444	106.43	-4.845	3
1.1389	38.69	0.01381	-0.005	112.6	4
2.0361	37.76	8.950-3 ^a	-8.046	-1.637	3
2.7767	37.00	1.274-3 ^a	62.366	-43.82	4
3.1566	38.00	0.02422	-82.492	17.706	3
3.6208	36.00	0.04129	-27.76	29.516	4
4.8508	35.97	0.07169	0.048	-3.828	4
5.4497	37.00	0.03840	-80.508	-369.36	4
6.2094	38.00	0.16621	-110.94	75.912	3
6.3913	36.71	0.25177	10.327	0.163	4
7.0860	38.54	0.14362	0.226	29.959	4
7.6394	38.00	4.768-3 ^a	104.92	155.15	3
8.7726	32.77	1.5832	27.581	-70.354	4
12.400	39.02	3.4064	-2.701	26.655	3
19.293	37.00	12.113	-5.849	57.741	4

^aRead 2.422-3 as 2.422×10^{-3} .

Table C-2. Adler-Adler resonance parameters

μ (eV)	ν (eV)	GT (b*eV ^{3/2})	HT (b*eV ^{3/2})	GF (b*eV ^{3/2})	HF (b*eV ^{3/2})	GC (b*eV ^{3/2})	HC (b*eV ^{3/2})
-99.9999	0.0614	658.2420	0.1097	388.1400	0.0596	208.6640	0.0279
-89.9993	0.1549	0.1827	0.0649	0.1596	0.0648	0.0231	0.
-4.2896	0.2382	2556.6499	2.4581	2329.7900	1.1530	188.3700	-0.4589
-3.4930	0.0288	0.0244	-0.0153	0.0052	-0.0152	0.0193	0.
-1.5036	0.0285	0.0111	-0.0795	-0.0448	-0.0767	0.0559	-0.0029
-0.4106	0.0933	133.3380	-1.7793	111.7600	-1.8025	21.4699	-0.0025
-0.1961	0.1180	-1.8762	-3.0185	-2.3741	-3.0592	0.5008	0.0395
-6.88-5 ^a	0.0157	-0.0041	0.0398	-0.0408	0.0382	0.0367	0.0016
0.2835	0.0749	4.7196	-1.2730	3.4821	-1.2670	1.2370	-0.0059
1.1422	0.0755	9.2286	3.0268	6.7055	3.0193	2.5204	0.0102
2.0362	0.0237	3.5922	0.0255	0.7362	0.0244	2.8553	0.0003
2.7757	0.0717	-0.0723	-1.1185	-0.3650	-1.1093	0.2925	-0.0092
3.1569	0.0692	7.7725	1.4761	5.6005	1.4741	2.1708	-0.0001
3.6183	0.0464	16.2850	2.8601	9.7871	2.8423	6.4907	0.0114
4.8512	0.0198	23.7335	0.5463	2.1320	0.5200	21.5586	0.0095
5.4488	0.2442	12.0009	-2.3868	11.0516	-2.3555	0.9438	-0.0407
6.2068	0.1125	38.3881	1.9092	31.8716	1.8957	6.4883	-0.0023
6.3908	0.0236	73.8810	0.1598	16.0678	0.0901	57.4141	-0.0071
7.0842	0.0342	39.8103	0.1244	17.1529	0.1042	22.5710	-0.0144
7.6382	0.1491	0.9453	0.4602	0.8122	0.4599	0.1333	-0.0001
8.7696	0.0660	393.7580	-19.7083	290.9340	-19.7250	98.0757	-0.1292
12.3996	0.0359	555.7460	-0.8336	227.1290	-0.7522	302.2380	-0.0006
19.2922	0.0563	2037.4600	16.9521	1148.9900	18.4169	669.3000	-0.4539

^aRead -6.88 - 5 as -6.88×10^{-5} .

The G's and H's include the constant $c = 652000$ b-eV and should be divided by that number to conform to ENDF/B-Format.

Table C-3. Multipole momentum space resonance parameters

μ (eV ^{1/2})	ν (eV ^{1/2})	GT (b*eV ^{3/2})	HT (b*eV ^{3/2})	GF (b*eV ^{3/2})	HF (b*eV ^{3/2})	GC (b*eV ^{3/2})	HC (b*eV ^{3/2})
-4.3923	-0.0050	1018.7400	10.3319	732.0140	9.2093	426.3620	0.0011
-3.5213	-0.0046	277.8730	-0.3156	125.4760	-0.3761	166.9700	0.
-2.9614	-0.0109	196.8870	-9.7987	149.0650	-9.8635	50.2484	0.
-2.7639	-0.0270	0.4728	0.2298	0.4061	0.2299	0.0666	0.
-2.6616	-0.0064	19.9048	0.0488	8.6136	0.0521	11.3346	0.
-2.5280	-0.0046	36.9420	0.0407	8.1232	0.0451	29.0206	0.0088
-2.4915	-0.0225	19.1944	0.9433	15.9597	0.9478	3.2490	0.
-2.3349	-0.0523	5.9977	-1.1971	5.5270	-1.1778	0.4726	-0.0185
-2.2025	-0.0045	11.8673	0.2673	1.0704	0.2600	10.8187	0.0084
-1.9022	-0.0122	8.1427	1.4303	4.8988	1.4213	3.2482	0.0079
-1.7769	-0.0195	3.8865	0.7371	2.8014	0.7371	1.0857	0.
-1.6662	-0.0215	-0.0360	-0.5593	-0.1825	-0.5547	0.1464	-0.0046
-1.4270	-0.0083	1.7962	0.0125	0.3683	0.0122	1.4282	0.0004
-1.0693	-0.0353	4.6134	1.5169	3.3540	1.5099	1.2606	0.0053
-0.5370	-0.0697	2.3600	-0.6360	1.7414	-0.6335	0.6187	-0.0028
-0.1280	-0.4609	-0.9374	-1.5103	-1.1873	-1.5298	0.2499	0.0199
-0.0883	-0.0887	-0.0020	-0.0199	-0.0204	0.0191	0.0184	0.0008
-0.0723	-0.6448	66.6587	-0.8975	55.9248	-0.9455	10.7438	-0.0053
-0.0566	-2.0710	1277.3000	0.5567	1182.4100	-17.4759	95.6056	-1.4892
-0.0116	-1.2263	0.0056	-0.0398	-0.0224	-0.0383	0.0280	-0.0014
-0.0082	-9.4868	0.0913	0.0324	0.0798	0.0324	0.0116	0.
-0.0077	-1.8690	0.0122	-0.0077	0.0026	-0.0076	0.0096	0.
-0.0028	-9.9997	329.0730	0.0298	211.8040	-21.7745	113.8660	-11.7220
0.0028	10.0003	329.1700	0.0298	211.8040	21.8341	113.8660	11.7220
0.0077	1.8690	0.0122	-0.0077	0.0026	-0.0076	0.0096	0.
0.0082	9.4868	0.0914	0.0324	0.0798	0.0324	0.0116	0.
0.0116	1.2263	0.0056	-0.0398	-0.0224	-0.0383	0.0280	-0.0014
0.0566	2.0728	1279.3300	0.5388	1182.4100	18.6291	95.6056	1.4315
0.0723	0.6449	66.6785	-0.8986	55.9247	-0.8571	10.7438	0.0117
0.0883	0.0887	-0.0020	0.0199	-0.0204	0.0191	0.0184	0.0008
0.1280	0.4609	-0.9371	-1.5093	-1.1871	-1.5298	0.2499	0.0200
0.5370	0.0698	2.3597	-0.6366	1.7411	-0.6335	0.6186	-0.0028
1.0693	0.0353	4.6143	1.5132	3.3528	1.5097	1.2603	0.0053
1.4270	0.0083	1.7961	0.0126	0.3681	0.0122	1.4276	0.0004
1.6662	0.0215	-0.0363	-0.5593	-0.1825	-0.5546	0.1464	-0.0046
1.7769	0.0195	3.8863	0.7377	2.8003	0.7371	1.0854	0.0003
1.9022	0.0122	8.1429	1.4279	4.8936	1.4212	3.2450	0.0078
2.2025	0.0045	11.8669	0.2694	1.0660	0.2600	10.7792	0.0084
2.3349	0.0523	6.0000	-1.1954	5.5258	-1.1777	0.4723	-0.0184
2.4915	0.0226	19.1942	0.9530	15.9358	0.9478	3.2441	0.0003
2.5280	0.0047	36.9405	0.0671	8.0339	0.0451	28.7070	0.0089
2.6616	0.0064	19.9051	0.0551	8.5764	0.0521	11.2855	-0.0002
2.7639	0.0270	0.4727	0.2301	0.4061	0.2299	0.0666	0.
2.9614	0.0111	196.8750	-9.9275	145.4660	-9.8624	49.0410	-0.0001
3.5213	0.0051	277.8730	-0.4363	113.5640	-0.3761	151.1190	0.0001
4.3923	0.0064	1018.7300	8.0880	574.4950	9.2084	334.6420	0.0010

The G's and H's include the constant $c = 652000$ b·eV.

APPENDIX D

RENORMALIZATION AND RESIDUAL BACKGROUND

Renormalization and residual background calculated with the computer code SAMMY are shown in Table D-1. Figure D-1 shows the effect of the residual background on the fission cross section data of Blons. The solid lines, in the upper and lower curves of Fig. D-1, represent the calculation with and without the residual background effect, respectively. The vertical lines are the data of Blons.

Table D-1. Renormalization and Residual Background

Data	Normalization	Background	Type of Background
Harvey et al. ³¹ (80 m) (0.03269 atom/b)	0.999	6.189-5 ^a	Constant
Harvey et al. ³¹ (80 m) (0.002355 atom/b)	1.0	8.003-4	Constant
Harvey et al. ³¹ (18 m) (0.03269 atom/b)	1.0	3.536-4	Constant
Weston and Todd ²⁶	0.996	6.392-2	Proportional to \sqrt{E}
Blons ²⁵	0.963	0.232	Proportional to \sqrt{E}
Gwin et al. ²⁸	1.0	0.021	Proportional to \sqrt{E}

^aRead 6.189-5 as 6.189×10^{-5} .

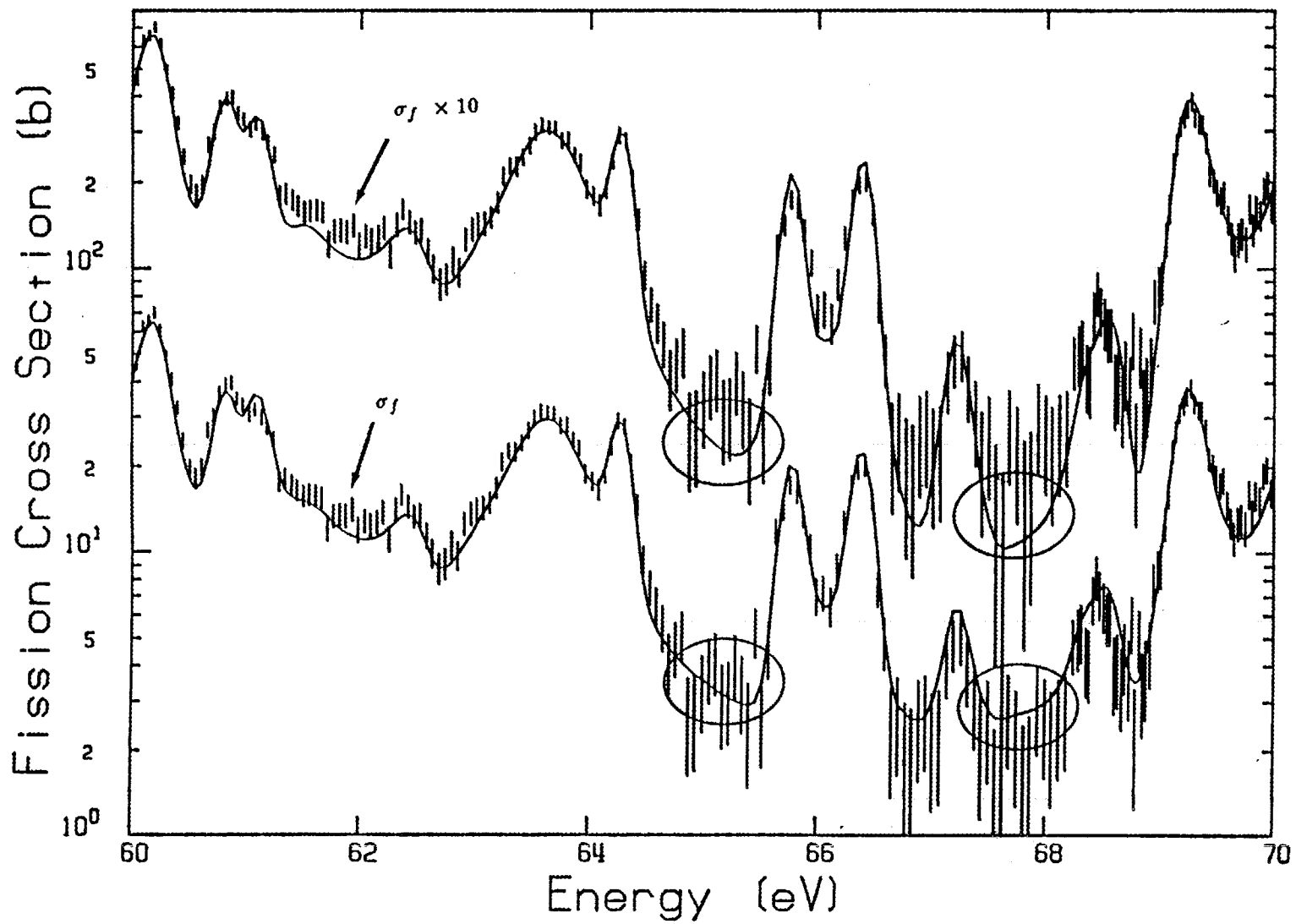


Fig. D-1. Residual background on the fission cross-section data of Blons.

INTERNAL DISTRIBUTION

- | | |
|-----------------------|---|
| 1. B. R. Appleton | 23. J. J. Dorning (consultant) |
| 2-6. G. de Saussure | 24. R. M. Haralick (consultant) |
| 7. F. Difilippo | 25. J. E. Leiss (consultant) |
| 8. D. M. Hetrick | 26. N. Moray (consultant) |
| 9. D. C. Larson | 27. M. F. Wheeler (consultant) |
| 10. N. M. Larson | 28. EPMD Reports Office |
| 11. R. L. Macklin | 29-30. Laboratory Records
Department |
| 12. F. C. Maienschein | 31. Laboratory Records,
ORNL-RC |
| 13. R. W. Peelle | 32. Document Reference
Section |
| 14. F. G. Perey | 33. Central Research Library |
| 15-19. R. B. Perez | 34. ORNL Patent Section |
| 20. R. R. Spencer | |
| 21. L. W. Weston | |
| 22. R. Q. Wright | |

EXTERNAL DISTRIBUTION

35. Office of the Assistant Manager for Energy, Research and Development, U.S. Department of Energy, Oak Ridge Operations, P. O. Box 2001, Oak Ridge, TN 37831
36. M. R. Bhat, Building 197D, National Nuclear Data Center, Brookhaven National Laboratory, Upton, NY 11973
37. R. C. Block, Department of Nuclear Engineering, Rensselaer Polytechnic Institute, Troy, NY 12181
38. C. Coceva, ENEA Comitato Nazionale, Centro Recherche Energie, Ezio Clemental, via G. Maxxini, 2, 40138, Bologna, Italy
39. R. P. Corcuera, Centro Tecnico Aeroespacial, Instituto de Estudos Avancados, Caixa Postal 6044, 72232 Sao José dos Campos, SP Brasil
40. C. Dunford, Building 197D, National Nuclear Data Center, Brookhaven National Laboratory, Upton, NY 11973
41. F. H. Fröhner, Institut für Neutronenphysik und Reaktortechnik, Kernforschungszentrum Karlsruhe, Postfach 3640, 7500 Karlsruhe, Federal Republic of Germany
42. Philip B. Hemmig, Chief, Physics Branch, Reactor Research and Technology, Office of Energy Technology, U.S. Department of Energy, Washington, DC 20545
43. R. N. Hwang, Argonne National Laboratory, Engineering Physics Division, Argonne, IL 60439
44. L. C. Leal, Argonne National Laboratory, 9700 South Cass Avenue, Argonne, IL 60439
45. E. C. Lynn, Nuclear Physics Division, Atomic Energy Research Establishment, Harwell, Didcot, Oxon, OX11, ORA, United Kingdom
46. R. E. MacFarlane, Los Alamos National Laboratory, P. O. Box 1663, Los Alamos, NM 87545
47. T. Nakagawa, Japan Atomic Energy Research Institute, Tokai Research Establishment, Linac Laboratory, Tokai-Mura, Naka-Gun, Ibaraki-Ken, Japan

48. S. Pearlstein, Brookhaven National Laboratory, Building 197D, National Nuclear Data Center, Upton, NY 11973
49. W. P. Poenitz, Argonne National Laboratory-West, P. O. Box 2528, Idaho Falls, ID 83403
50. P. Ribon, C.E.N. Saclay, Departement des Etudes Mécaniques et thermiques, BP2, 91190, Gif-sur-Yvette, France
51. M. Salvatore, Commissariat à l'Energie Atomique, Centre d'Etudes Nucleaires de Cadarache, Boite Postale No. 1, 13115 Saint-Paul-Lez-Durance, France
52. Donald L. Smith, Building 314, Engineering Physics Division, Argonne National Laboratory, 9700 South Cass Ave., Argonne, IL 60439
53. M. G. Sowerby, Nuclear Physics Division, Building 418, Atomic Energy Research Establishment, Harwell, Didcot, Oxon, OX11, ORA, United Kingdom
54. C. Wagemans, Central Bureau for Nuclear Measurements, Steenweg naar Retie, B-2400, Geel, Belgium
55. Herman Weigmann, Central Bureau for Nuclear Measurements, Steenweg naar Retie, B-2400, Geel, Belgium
56. S. L. Whetstone, Division of Nuclear Physics, Office of Energy Research, U.S. Department of Energy, Room G-315, Washington, DC 20545
57. Roger White, Lawrence Livermore National Laboratory, P. O. Box 808, Livermore, CA 94550
- 58-67. Office of Scientific and Technical Information, P. O. Box 62, Oak Ridge, TN 37831